A Miniaturized Thin-Plate Low Cycle Fatigue Test Method at Elevated Temperature

Li M.[1], Maskill S.[2], Wen Z.X.[1], Yue Z.F.[1], and Sun W.[2]

[1]Northwestern Polytechnical University School of Mechanics Civil Engineering and Architecture
[2]University of Nottingham Faculty of Engineering

October 30, 2021

Abstract

This study aims to develop a high temperature LCF test method using a non-standard miniature thin-plate (MTP) specimen in order to characterize cyclic visco-plasticity behavior of component materials. For demonstration, fully reversed strain-range controlled LCF and creep-fatigue (CF) tests at 600 °C have been performed for a martensitic steel using both standard-sized full-scale (SSFS) and MTP specimens. A scaling factor is determined using cyclic visco-plastic finite element (FE) for geometry constraint evaluation and data conversion based on the reference strain approach. The equivalent energy principal is proposed to assess the geometry constraint effect that non-standard MTP specimen has. The high temperature LCF results from the MTP specimen based on the proposed testing methodology have shown a good agreement with SSFS specimen data under equivalent conditions. The methodology can therefore be used to conduct accurate transferability to achieve equivalent LCF behavior between the conventional standard specimen and the MTP specimen.

A Miniaturized Thin-Plate Low Cycle Fatigue Test Method at Elevated Temperature

M., Li[1,2]*, S., Maskill[2], Z.X., Wen[1], Z.F., Yue[1], W., Sun[2]

[1]School of Mechanics, Civil Engineering and Architecture, Northwestern Polytechnical University, Xi'an, 710072, China

[2]Faculty of Engineering, University of Nottingham, Nottingham, NG72RD, UK

Abstract: This study aims to develop a high temperature LCF test method using a non-standard miniature thin-plate (MTP) specimen in order to characterize cyclic visco-plasticity behavior of component materials. For demonstration, fully reversed strain-range controlled LCF and creep-fatigue (CF) tests at 600 °C have been performed for a martensitic steel using both standard-sized full-scale (SSFS) and MTP specimens. A scaling factor is determined using cyclic visco-plastic finite element (FE) for geometry constraint evaluation and data conversion based on the reference strain approach. The equivalent energy principal is proposed to assess the geometry constraint effect that non-standard MTP specimen has. The high temperature LCF results from the MTP specimen based on the proposed testing methodology have shown a good agreement with SSFS specimen data under equivalent conditions. The methodology can therefore be used to conduct accurate transferability to achieve equivalent LCF behavior between the conventional standard specimen and the MTP specimen.

Keywords: *MTP; SSFS; LCF; Unified Visco-Plasticity Model; Scaling Factor*

Corresponding Author:**ming.li1@nwpu.edu.cn***

Nomenclature

	the length of the parallel gauge length section
	the width of the parallel gauge length section
	fillet radius
w	the width of MTP specimen
	total strain tensor
	elastic strain tensor
	visco-plastic strain tensor
	Cauchy stress tensor
,	identity tensor and deviatoric part
	shear and bulk moduli
	the second invariant
	von-Mises yield function
	the deviatoric stress of Cauthy stress tensor
,	non-linear kinematic hardening back-stress, deviatoric part of back-stress
	later and initial kinematic hardening back-stress
	isotropic hardening drag stress
	visco-plastic multiplier
	visco-plastic multiplier rate
	initial cyclic yield stress
	linear hardening term
	dynamic recovery term
,	kinematic hardening parameters
,	isotropic hardening parameters
	total effective gauge length
	scaling factor
	intended applied displacement
	displacement between the parallel gauge length
	average strain between the parallel gauge length
	hysteresis area
	Young's modulus
n'	cyclic strain hardening exponent
K'	cyclic strength coefficient
N, N_f	number of cycles, and number of cycles to failure

1. Introduction

High temperature thermal systems such as power plant steam piping work and gas turbines[1], chemical plant pressure vessels[2-3], aero-engine combustion structures[4], etc., may fail due to accumulated damage caused by long-term creep, fatigue, CF under elevated temperature. In engineering applications, it is always inevitably required to precisely evaluate the material properties, residual life of in-service components, which has led to the development of non-destructive or "quasi" non-destructive technique. On the basis of these demands, various small-sized, miniature specimen techniques have been developed[5-8] and are being increasingly used to assist in condition minoring and life management programs[9-11]. In order to obtain comparable constitutive behavior as SSFS specimen, there are three critical issues on the development of miniaturized testing: i) the standardization for high temperature LCF miniature specimens for sub-sized thin structures, e.g., coating-substrate systems[12-13] or narrow heat-affected zones (HAZs)[2,14], ii) improvements in LCF testing apparatus leading to high accuracy test rigs, and iii) robust mechanics-based theoretical methods for LCF data transferability and correlation.

Data from small specimen creep testing has a direct input into remaining life evaluation and has become increasingly attractive for power plant application[11,15]. Such data can also be used to generate creep constitutive laws for welded materials[14,16,17]. The main small specimen and testing types that are used to obtain high temperature tensile and creep properties include the conventional sub-sized uniaxial specimens[18] and several specialized miniature specimen test types including: the impression creep test[19-21], the small punch tensile, creep and fracture tests[22-26], the small ring creep test[27-29], the small tensile two bar creep test[30], and the more recent miniature thin-plate tensile test[12,13,31]. One of the unique advantages that small punch creep test has is the very small thickness (~ 0.5 mm), however, there is no universally accepted conversion techniques available for data interpretation[32,33]. Recently, small punch related constitutive model was developed to predict the uniaxial tensile stress-strain response of materials based on an energy principle, which was capable to accurately convert the load-displacement data into stress-strain description[34]. In addition, instrumented indentation test (IIT) was applied in remaining life assessment, a good agreement was obtained between the standard specimens and the numerical prediction[35]. Impression creep testing requires a small amount of material to only produce steady-state creep data after a transient primary stage, which is attractive in the localized deformation and damage behavior[36-37]. The two-bar specimen can produce the full stage creep curves, but it is difficult to make it very thin to ensure that the two bars fail at the same time[30]. Inverse approaches[33,38-39]have been adopted in miniaturized beam/thin-plate bending specimen/small punch creep tests to obtain creep properties, based on analytical solutions and numerical modelling.

Up to date, most of the research focus on the miniaturized creep tests, however, there has been a significant missing gap in small specimen LCF test as many issues are still waiting for the technical solutions[40-42]. For example, almost all the testing approaches, such as testing rigs and gripping fixtures, are specially designed for the standard specimens. Moreover, the miniature specimens are apt to suffer from torsional damage during high temperature cyclic testing. In the recent years, cylindrical small-sized specimens had been successfully applied on LCF tests by Dzugan *et al* .,[41,42], which were not compared and validated by the standard specimen tests. Small punch high cycle fatigue tests had been conducted on Ti-6Al-4V[43,44], however, it was very difficult to derive stress-strain hysteresis response. An alternative miniature fatigue test method, using a thin-plate specimen, could provide a much more reliable fatigue data. For example, LCF tests were carried out by Nozaki *et al.,* and Nogami *et al.* ,[45,46] using round bar and thin-plate specimens, and little difference was found in LCF behavior. Thermal-mechanical fatigue tests were performed on Ni-based superalloy, and the results showed good agreement of the fatigue lives between miniature and conventional specimen tests[47]. Although the miniature LCF testing mentioned above has paved the way for evaluating the cyclic properties and is capable to represent cyclic plasticity behavior of SSFS specimen using a relatively long enough gauge length[45-47], more extensive investigations on LCF and CF with smaller-sized specimens at higher temperature are still scare before standardization of the testing methods.

The current work proposes a new experimental and numerical framework for non-standard MTP specimen, which aims to duplicate the LCF behavior of SSFS specimen at elevated temperature. The organization of the paper is as follows: the experimental methodology is presented in Section 2, consisting of material, specimen design, experimental set-up, and comparisons of uniaxial tensile responses between SSFS and MTP specimens. A high temperature unified visco-plasticity (UVP) modelling framework is introduced in Section 3 including data interpretation. The comparisons of high temperature LCF testing results between MTP and SSFS testing are presented in Section 4, followed by detailed discussions and future technical improvements in Section 5.

2. Experimental Methodology

2.1 Material and Test Program

The material used for both MTP and SSFS specimen tests is a martensitic FV566 steel extracted from an area close to the centerline of a gas turbine rotor, where it was service-aged for approximately 90,000 h at ~ 420 °C at a maximum speed of 3000 rpm. The chemical compositions of the material are (wt.%): C-0.6; Si-0.038; Mn-0.668; Cr-11.9; Mo-1.68; Ni-2.52; V-0.298; S-0.006 and Fe-remainder.

Uniaxial tensile, fully reversed saw-tooth, and hold-dwell LCF tests with a strain-rate of $0.01\%s^{-1}$ until failure were carried out for SSFS specimens previously[1]. The geometry and dimension of the SSFS specimen with a

5 mm gauge diameter and a 10 mm gauge length is shown in Fig.1a. All the strain-controlled LCF tests and CF tests were conducted at 600 degC under a total strain-range of +- 0.7% using the two prescribed loading conditions, i.e., saw-tooth (Fig.1b) and dwell-type (Fig.1c) waveforms. A symmetrical triangular waveform (push-pull load ratioR_e = -1) was employed for the saw-tooth loading, and a trapezoidal waveform for the dwell-type loading. For dwell-type tests, the dwell period duration was imposed at the maximum tensile strain for a period of 2.5 hours for the first cycle and 5 mins for all the subsequent cycles. The dwell duration was chosen after careful investigation of the stress relaxation times (i.e., the 5 mins hold period was enough to reach the quasi-equilibrium state of the viscous stress). The high temperature LCF and CF tests for SSFS specimens were carried out on a Tinius Olsen H25KS electromechanical testing machine. More information about the testing can be found in the refs[1,3,49].

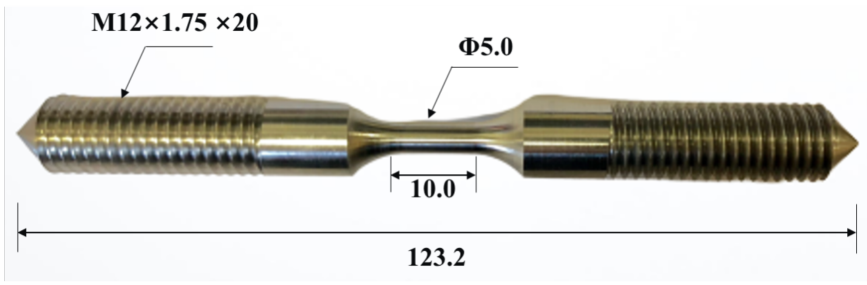

(a)

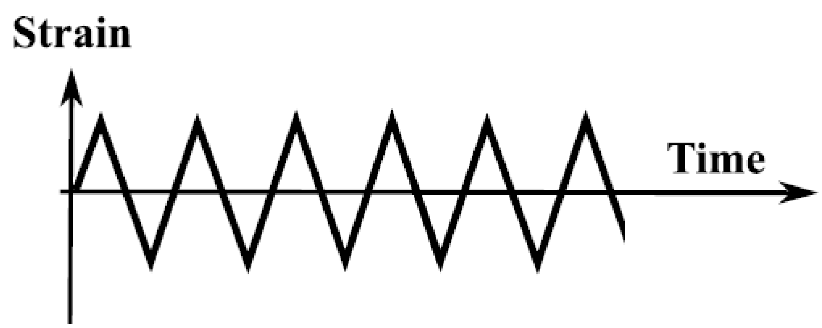

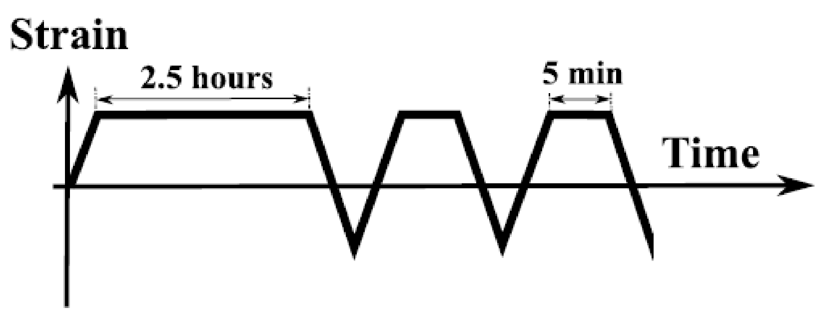

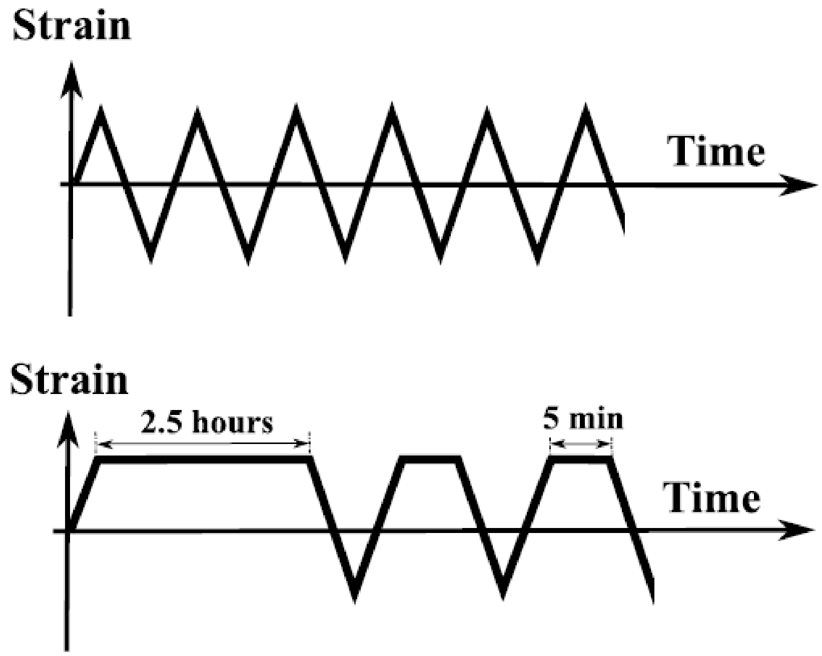

(b) (c)

Figs.1: (a) Geometry and dimension of FV566 SSFS uniaxial round bar specimen used for uniaxial tensile, high temperature LCF and CF testing (All measures given in mm); (b) conventional LCF saw-tooth profile; (c) CF dwell-type with initial tensile hold pattern for 2.5hours, and 5mins hold period for the subsequent cycles.

2.2 Non-Standard MTP Specimen Design, Test Rig and Experimental Set-Up

Fig.2a shows the geometry and dimension of the non-standard MTP specimens designed for high temperature LCF and CF tests. Thus, three values of l_0/d_0 were chosen, i.e., $l_0/d_0 = 1.0$ (MTP-1), $l_0/d_0 = 1.5$ (MTP-2), and $l_0/d_0 = 2.0$ (MTP-3), with the constant values, such as thickness (t = 0.5 mm), gauge width (d_0 = 1.0 mm), total width (w = 2.0 mm), and fillet radius (r = 2.0 mm). It should be mentioned that for the MTP specimens, size effect[50-52]in the thickness direction should be considered. Based on the previous findings in the refs[51-52], the number of grains in the thickness direction should exceed at least 5 ~ 6 grains in order to minimize the size effect, which is the basic principle for designing the thickness of MTP specimen in this study. According to the measured prior austenite grain size reported in the previous work[1], there are approximate 10 grains in the thickness direction. The MTP specimens with differentl_0/d_0 values are shown in Fig.2b. The loading assembly and experimental set-up is shown in Fig.2c, where the loading assembly is made of Nimonic 80. The polished MTP specimen is clamped at both ends by specially designed and manufactured clamps with machined rough surfaces to minimize the misalignment, strengthen the grip and reduce the slippage, see Fig.2d. The displacement is measured by two linear variable displacement transducers (LVDT) connected to both sides of the loading part of the machine.

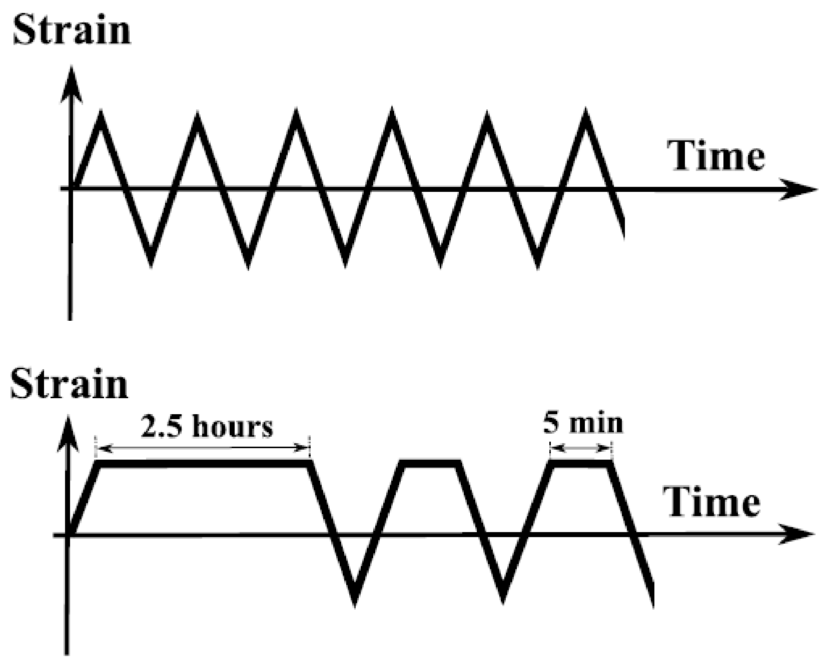
Strain
Time
Strain
2.5 hours
5 min
Time

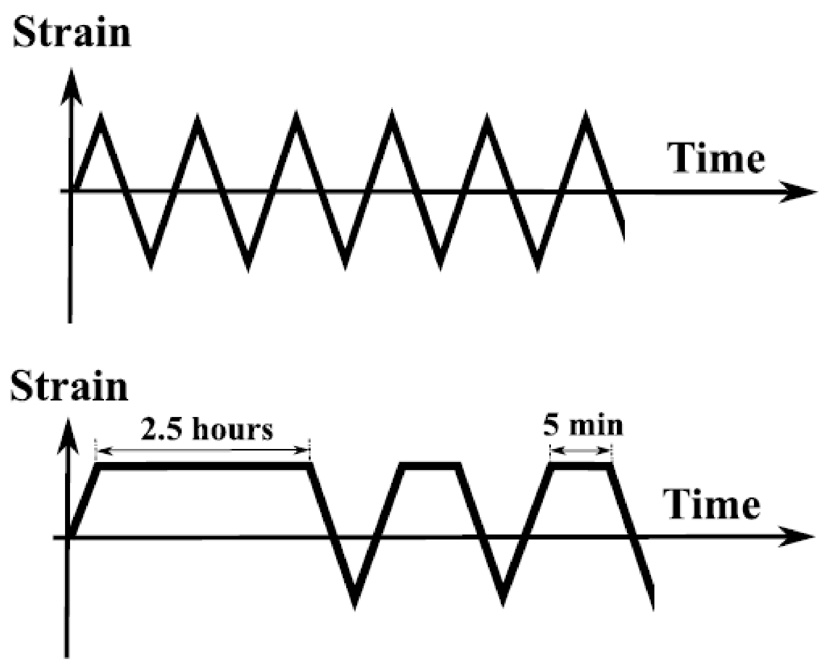
Strain
Time
Strain
2.5 hours
5 min
Time

(b)

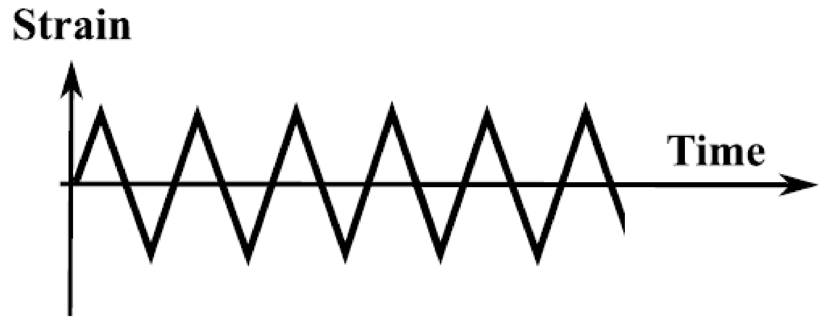

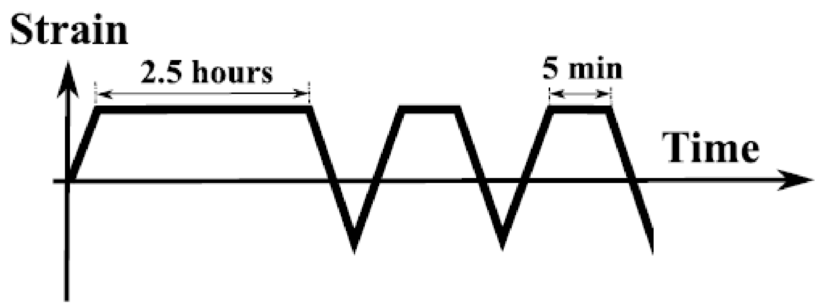

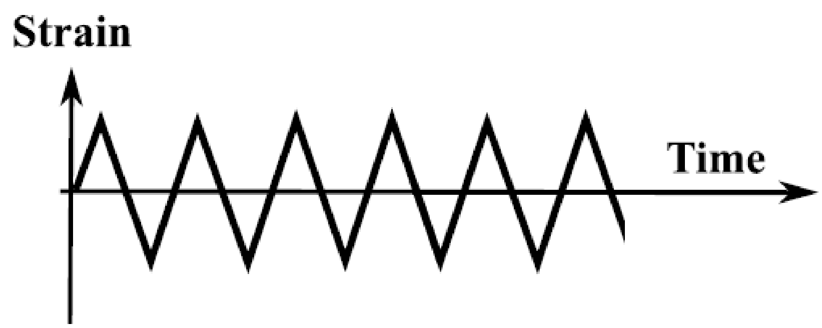

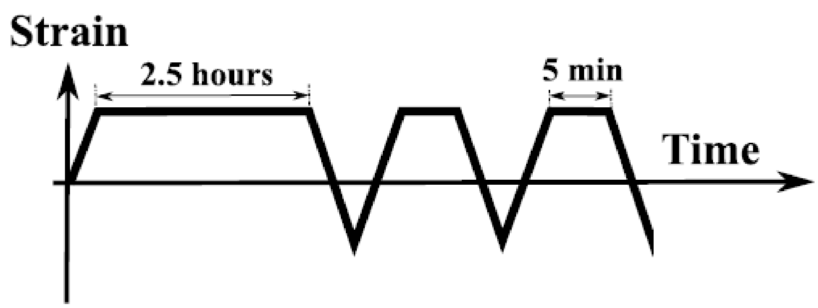

(c) (d)

Figs.2: (a) Geometry and dimension of MTP specimen for high temperature tensile, LCF and CF testing, (b) Three proposed MTP specimens with different gauge length to width ratios:$l_0/d_0 = 1.0$ (MTP-1),$l_0/d_0 = 1.5$ (MTP-2), and$l_0/d_0 = 2.0$ (MTP-3); (c) The Tinius Olsen H25KS single column high temperature testing machine; and (d) The specially designed loading assembly made of Nimonic 80 for the MTP cyclic test.

2.3 Uniaxial Tensile Test of MTP and SSFS specimens

Prior to high temperature LCF testing, uniaxial tensile test had been performed on MTP-3 and compared with SSFS testing results at 20 °C and 600 °C, respectively, in order to demonstrate the capability of the testing technique. The miniature uniaxial tensile tests were conducted using the testing rig as introduced in Section 2.2 (see Fig.2c). The applied displacement-rate for the MTP-3 specimen was under a constant of strain-rate of 0.01%s^{-1} during the tensile testing, which is consistent with the loading process of the SSFS tensile testing[1]. The applied torque on both screw bolts were keep the same with a value of 0.5Nm to avoid any torsions during testing and provide enough clamping force. Noted that the displacements were measured at the ends of the fillet radius regions since it is difficult to accommodate the extensometers into the very limited region. As can be seen from the testing results in terms of engineering stress-strain curves estimated from the initial cross-section area and displacement shown in Fig.3, the tensile responses from MTP-3 specimen follow the typical temperature-dependent stress-strain behaviors, for example, higher ultimate tensile response and lower ductility at 20 °C compared with these at 600 °C. More importantly, almost identical trend can be achieved, which indicates the possibility to make the comparisons of high temperature LCF and CF tests between MTP and SSFS specimens.

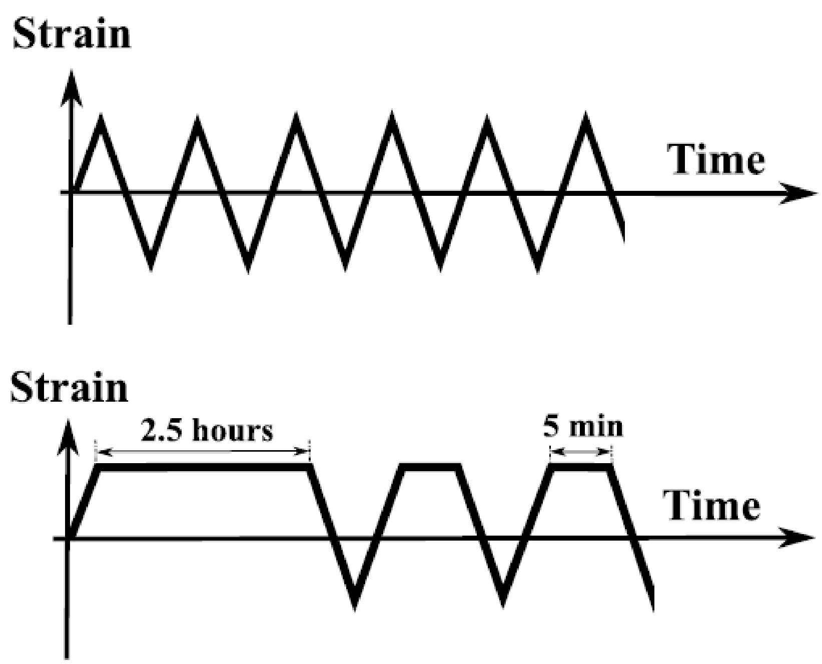

Fig.3: Comparison of engineering stress-strain responses obtained from the MTP-3 tensile tests and SSFS tensile test for FV566 at 20 °C and 600 °C, respectively. Good agreement was achieved, indicating the feasibility of the high temperature LCF tests for MTP specimen.

3. Theoretical Modelling and Data Interpretation

3.1 High Temperature Unified Visco-Plasticity Model

3.1.1 Constitutive Equations

In consideration of the geometry constraint effect that non-standard specimen has, it is necessary to correctly carry out the correlation evaluation using scaling factor between standard and non-standard small-sized specimens in advance[15,53-55], otherwise, the applied displacement on MTP specimen for representing SSFS testing data will be under- or over- estimated, leading to a large amount of inaccuracy in cyclic plasticity property evaluation. According to the latest literature review, the authors have not yet noticed any published work on this topic using finite element (FE) modelling approach to evaluate scaling factor based on an advanced mechanics-based material model, especially in high temperature LCF testing for non-standard small-sized thin-plate specimen.

Hosted file

`image41.wmf` available at https://authorea.com/users/443699/articles/543644-a-miniaturized-thin-plate-low-cycle-fatigue-test-method-at-elevated-temperature

Hosted file

`image42.wmf` available at https://authorea.com/users/443699/articles/543644-a-miniaturized-thin-plate-low-cycle-fatigue-test-method-at-elevated-temperature

Hosted file

`image43.wmf` available at https://authorea.com/users/443699/articles/543644-a-miniaturized-thin-plate-low-cycle-fatigue-test-method-at-elevated-temperature

The Chaboche type UVP material model[1,3,49] is adopted in this work, to describe the high temperature, cyclic visco-plastic behavior of FV566 steel. The basis for choosing such a model is that the overall high temperature cyclic behavior is a combination of rate-dependent cyclic plasticity and temperature-dependent creep, which can be well described by Chaboche UVP model, in which, the total deformation is simply assumed to consist of elastic and inelastic (visco-plastic) components, where the latter is a combination of creep and cyclic plasticity. Hence, under small-strain deformation, the total strain tensor,, is composed of both a small recoverable elastic strain tensor,, and a large irreversible visco-plastic strain tensor,, such that:

Hosted file

`image44.wmf` available at https://authorea.com/users/443699/articles/543644-a-miniaturized-thin-plate-low-cycle-fatigue-test-method-at-elevated-temperature

(1)

Hosted file

`image45.wmf` available at https://authorea.com/users/443699/articles/543644-a-miniaturized-thin-plate-low-cycle-fatigue-test-method-at-elevated-temperature

According to Hooke's law, the elastic strain is linked to the Cauchy stress tensor,, which can be determined through the following relation for isotropic material, such that:

Hosted file

`image46.wmf` available at https://authorea.com/users/443699/articles/543644-a-miniaturized-thin-plate-low-cycle-fatigue-test-method-at-elevated-temperature

(2)

Hosted file

`image47.wmf` available at https://authorea.com/users/443699/articles/543644-a-miniaturized-thin-plate-low-cycle-fatigue-test-method-at-elevated-temperature

Hosted file

`image48.wmf` available at https://authorea.com/users/443699/articles/543644-a-miniaturized-thin-plate-low-cycle-fatigue-test-method-at-elevated-temperature

Hosted file

image49.wmf available at https://authorea.com/users/443699/articles/543644-a-miniaturized-thin-plate-low-cycle-fatigue-test-method-at-elevated-temperature

Hosted file

image50.wmf available at https://authorea.com/users/443699/articles/543644-a-miniaturized-thin-plate-low-cycle-fatigue-test-method-at-elevated-temperature

Hosted file

image51.wmf available at https://authorea.com/users/443699/articles/543644-a-miniaturized-thin-plate-low-cycle-fatigue-test-method-at-elevated-temperature

Hosted file

image52.wmf available at https://authorea.com/users/443699/articles/543644-a-miniaturized-thin-plate-low-cycle-fatigue-test-method-at-elevated-temperature

Hosted file

image53.wmf available at https://authorea.com/users/443699/articles/543644-a-miniaturized-thin-plate-low-cycle-fatigue-test-method-at-elevated-temperature

Hosted file

image54.wmf available at https://authorea.com/users/443699/articles/543644-a-miniaturized-thin-plate-low-cycle-fatigue-test-method-at-elevated-temperature

whereand stand for the shear and bulk moduli, and

is the deviatoric part of the fourth-rank identity tensor, . The current UVP model includes both non-linear kinematic hardening back-stresses, , related to the motion of center of yield surface, and isotropic hardening drag stress, , related to the yield surface expansion, after cyclic plastic deformation. Thus, the inelastic visco-plastic strain-rate flow rule,, based on the von-Mises yield function, , can be assumed to be independent of hydrostatic pressure and defined such that:

Hosted file

image55.wmf available at https://authorea.com/users/443699/articles/543644-a-miniaturized-thin-plate-low-cycle-fatigue-test-method-at-elevated-temperature

(3)

Hosted file

image56.wmf available at https://authorea.com/users/443699/articles/543644-a-miniaturized-thin-plate-low-cycle-fatigue-test-method-at-elevated-temperature

(4)

Hosted file

image57.wmf available at https://authorea.com/users/443699/articles/543644-a-miniaturized-thin-plate-low-cycle-fatigue-test-method-at-elevated-temperature

Hosted file

image58.wmf available at https://authorea.com/users/443699/articles/543644-a-miniaturized-thin-plate-low-cycle-fatigue-test-method-at-elevated-temperature

Hosted file

image59.wmf available at https://authorea.com/users/443699/articles/543644-a-miniaturized-thin-plate-low-cycle-fatigue-test-method-at-elevated-temperature

Hosted file

image60.wmf available at https://authorea.com/users/443699/articles/543644-a-miniaturized-thin-plate-low-cycle-fatigue-test-method-at-elevated-temperature

where represents the initial cyclic yield stress. Following the normality assumption of visco-plasticity, the rate of visco-plastic strain, , is normal to the tangent to yield surface while its magnitude is identical to the inelastic visco-plastic multiplier rate, . The second invariant

is defined such that:

Hosted file

image61.wmf available at https://authorea.com/users/443699/articles/543644-a-miniaturized-thin-plate-low-cycle-fatigue-test-method-at-elevated-temperature

(5)

Hosted file

image62.wmf available at https://authorea.com/users/443699/articles/543644-a-miniaturized-thin-plate-low-cycle-fatigue-test-method-at-elevated-temperature

Hosted file

image63.wmf available at https://authorea.com/users/443699/articles/543644-a-miniaturized-thin-plate-low-cycle-fatigue-test-method-at-elevated-temperature

Hosted file

image64.wmf available at https://authorea.com/users/443699/articles/543644-a-miniaturized-thin-plate-low-cycle-fatigue-test-method-at-elevated-temperature

Hosted file

image65.wmf available at https://authorea.com/users/443699/articles/543644-a-miniaturized-thin-plate-low-cycle-fatigue-test-method-at-elevated-temperature

Hosted file

image66.wmf available at https://authorea.com/users/443699/articles/543644-a-miniaturized-thin-plate-low-cycle-fatigue-test-method-at-elevated-temperature

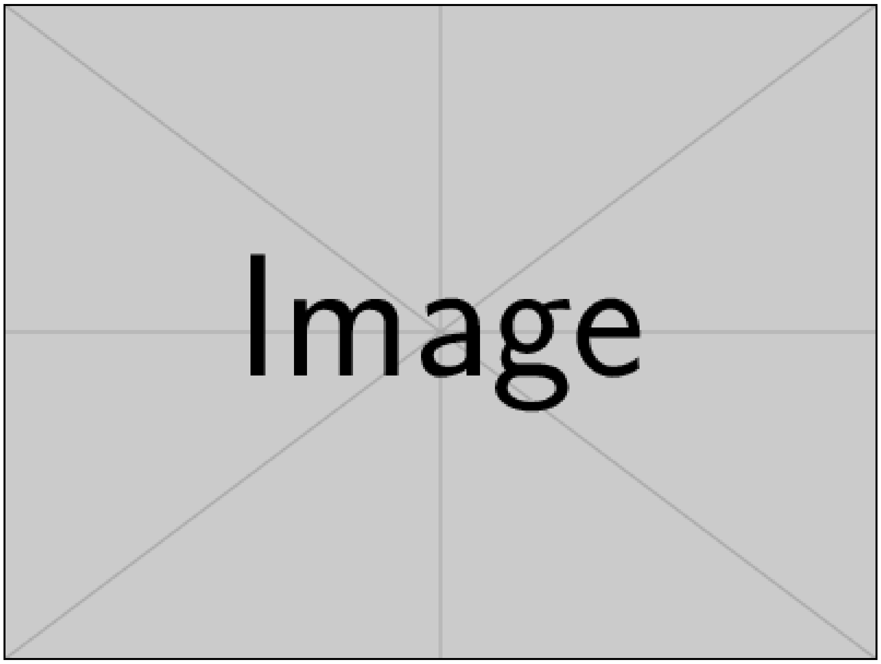

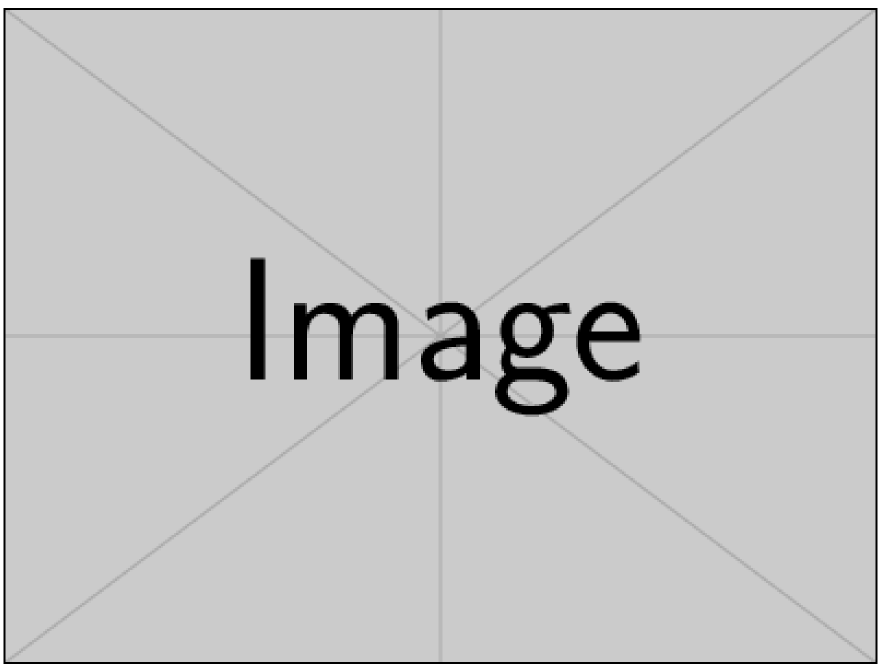

Hosted file

`image67.wmf` available at https://authorea.com/users/443699/articles/543644-a-miniaturized-thin-plate-low-cycle-fatigue-test-method-at-elevated-temperature

Hosted file

`image68.wmf` available at https://authorea.com/users/443699/articles/543644-a-miniaturized-thin-plate-low-cycle-fatigue-test-method-at-elevated-temperature

where is the deviatoric stress of Cauthy stress tensor. is the deviatoric part of the back-stress, , which can be further decomposed into two components,

and , to account for the Bauschinger effect[56], whilerepresents the initial kinematic hardening produced after the elastic portion, andaccounts for the kinematic hardening due to the later stage of strain hardening. An Armstrong-Frederick[56] form has been used to describe the non-linear evolution of the kinematic hardening, including linear hardening term,, and dynamic recovery term, . The Chaboche kinematic hardening decomposition of the elementary back-stress is formulated, as follows:

Hosted file

`image69.wmf` available at https://authorea.com/users/443699/articles/543644-a-miniaturized-thin-plate-low-cycle-fatigue-test-method-at-elevated-temperature

(6)

Hosted file

`image70.wmf` available at https://authorea.com/users/443699/articles/543644-a-miniaturized-thin-plate-low-cycle-fatigue-test-method-at-elevated-temperature

(7)

Hosted file

`image71.wmf` available at https://authorea.com/users/443699/articles/543644-a-miniaturized-thin-plate-low-cycle-fatigue-test-method-at-elevated-temperature

(7.1)

Hosted file

`image72.wmf` available at https://authorea.com/users/443699/articles/543644-a-miniaturized-thin-plate-low-cycle-fatigue-test-method-at-elevated-temperature

(7.2)

Hosted file

`image73.wmf` available at https://authorea.com/users/443699/articles/543644-a-miniaturized-thin-plate-low-cycle-fatigue-test-method-at-elevated-temperature

Hosted file

`image74.wmf` available at https://authorea.com/users/443699/articles/543644-a-miniaturized-thin-plate-low-cycle-fatigue-test-method-at-elevated-temperature

Hosted file

`image75.wmf` available at https://authorea.com/users/443699/articles/543644-a-miniaturized-thin-plate-low-cycle-fatigue-test-method-at-elevated-temperature

whereand

are kinematic hardening constants. A non-linear isotropic hardening stress, , is employed to account for the continuous decelerated cyclic softening, such that:

Hosted file

`image76.wmf` available at https://authorea.com/users/443699/articles/543644-a-miniaturized-thin-plate-low-cycle-fatigue-test-method-at-elevated-temperature

(8)

in which c and d are isotropic hardening parameters. This term represents the saturated value of the isotropic softening stress with increasing visco-plastic multiplier and the decay-rate, d , that leads to the softening saturation, c . The UVP model has been numerically implemented in ABAQUS FE user subroutine UMAT using an implicit integration scheme[1,3,49].

3.1.2 Determination and Calibration of the Model Parameters

The cyclic constitutive parameters identification used in the UVP model are conducted on the cyclic plasticity test data from the high temperature uniaxial LCF tests on SSFS specimen at 600 °C for FV566[1]. The UVP model adopted in this work employs 8 parameters in total. The determination of the material parameters follows a step-by-step procedure, with elastic parameter determined initially and followed by the remaining isotropic hardening and kinematic hardening parameters. The parameter d in Eq. (8) can be evaluated through the slope in the regression of the plot, while$c$ is determined from the difference in maximum stresses between the first and the saturated cycle using the SSFS experimental LCF data at 600 °C, as illustrated in Fig.4a. The SSFS experimental LCF data at 600 °C from the tensile part of the initial cycle and the corresponding regression fitting curves are provided in Fig.4b, illustrating the derivations of kinematic hardening parameters, a_n and b_n in Eq. (7.1). More detailed information about the total procedures of how to obtain the initial guess of the UVP parameters can be found in the author's previous work[1-3,49]. These initial parameters are then regarded as the starting points to obtain the optimized parameters using a first order non-linear least square minimization[1,3], where the minimum in the difference between the numerical and the experimental results is sought using two objective functions, i.e., i) experimental hysteresis loop of every cycle, and ii) experimental cyclic softening curve. The total set of the optimized UVP parameters for the FV566 at 600 °C is given in Table 1.

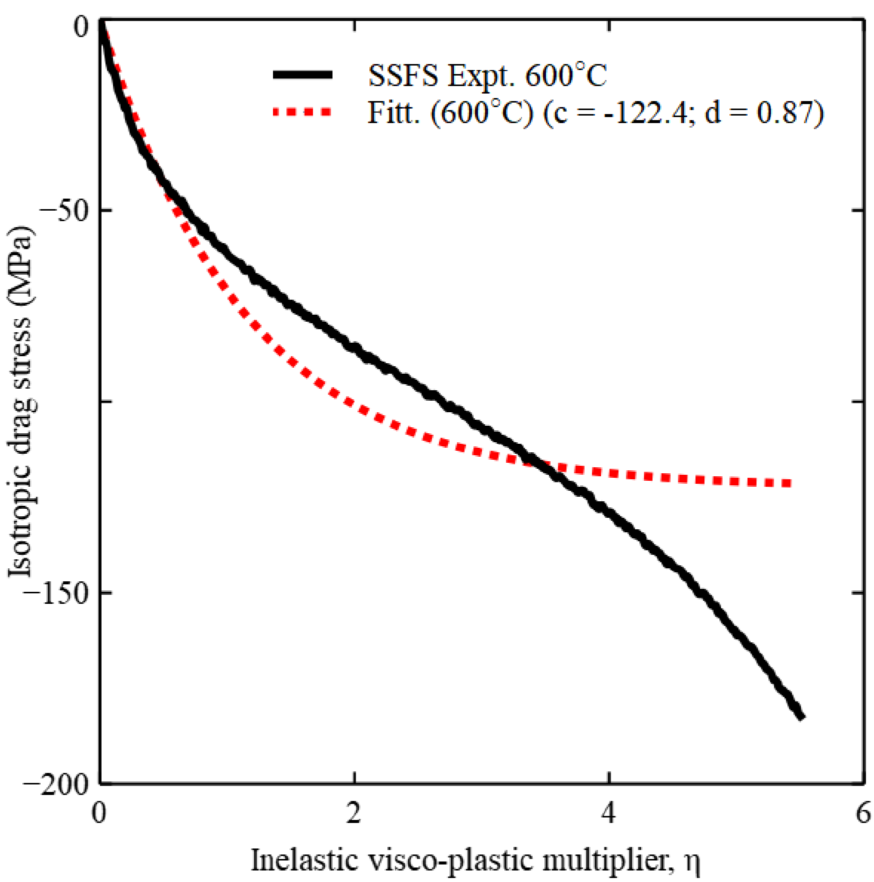

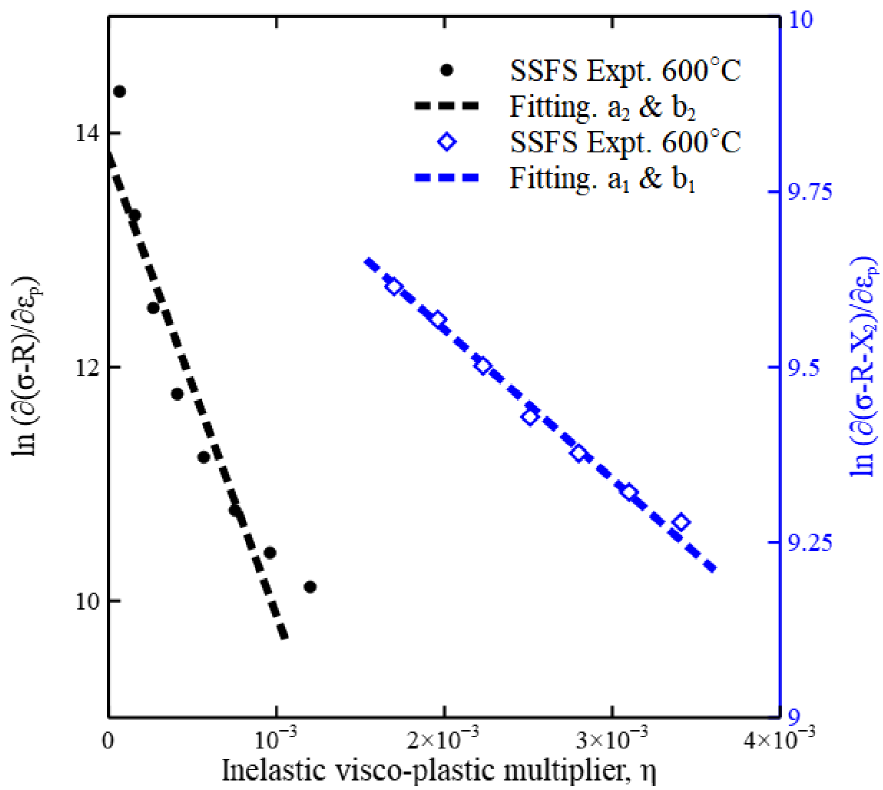

(b)

Figs.4: The determination of (a) isotropic parameters c and$d$ by fitting of drag stress evolution to describe the yield surface expansion with plastic deformation, and (b) kinematic parametersa_n and b_n for description of the movement of yield surface after material comes into yielding using SSFS high temperature LCF test data for FV566 at 600 .

Table 1: Optimized material parameters in the UVP model for FV566 at 600 .

Parameter scopes	Material parameters	Values
Elastic	Young's Modulus, E (MPa)	120850
	Initial cyclic yield stress, (MPa)	168.41
Isotropic & Kinematic hardening	Saturated softening stress, c (MPa)	-122.43
	Softening decay-rate, d (-)	0.87
	Back-stress-1, a_1 (MPa)	128.61
	Rate of decay-1, b_1 (-)	806.02
	Back-stress-2, a_2 (MPa)	643.63
	Rate of decay-2, b_2 (-)	126.36

Uniaxial cyclic visco-plasticity analysis using the UVP model is conducted using the home-made UMAT on a one-element cube model in ABAQUS, in conjunction with the optimized material parameters for calibration of SSFS experimental LCF data at 600 °C for FV566. The calibration procedure is achieved through the comparison between the predicted stress-strain hysteresis loop and experimentally measured SSFS uniaxial high temperature LCF data for a strain-rate of 0.01%s^{-1} and an applied strain-range of ± 0.7%. The results in Fig.5a illustrates an excellent agreement between the calibrated model and the experimental data at the initial cycle. The good comparison of the predicted and measured cyclic softening behavior is presented in Fig.5b.

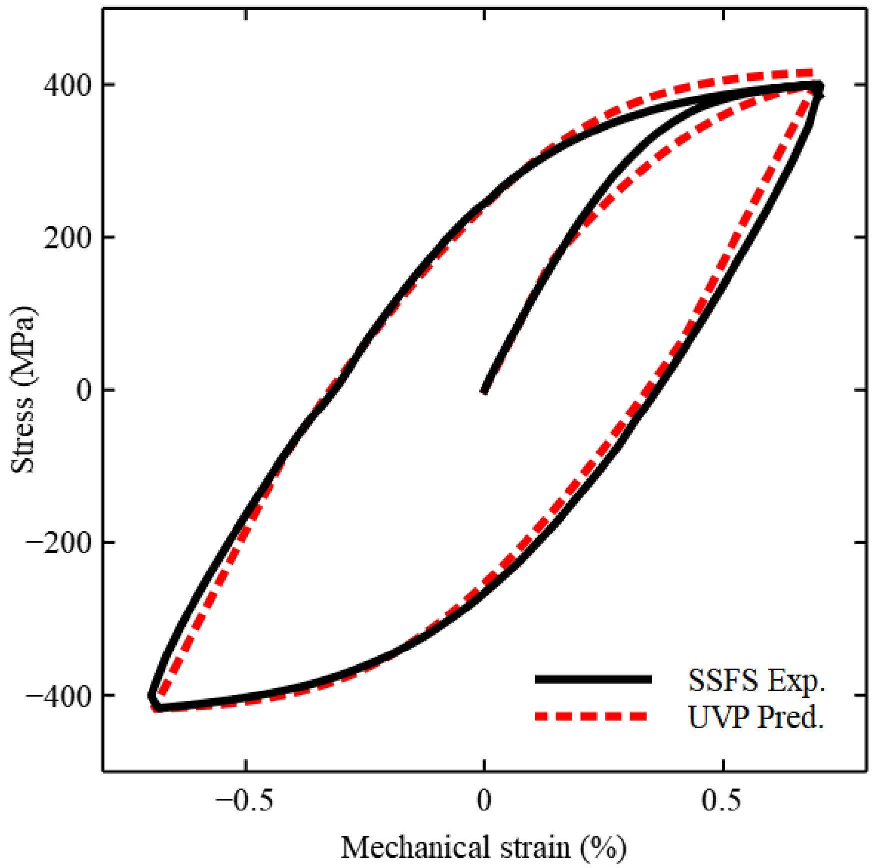

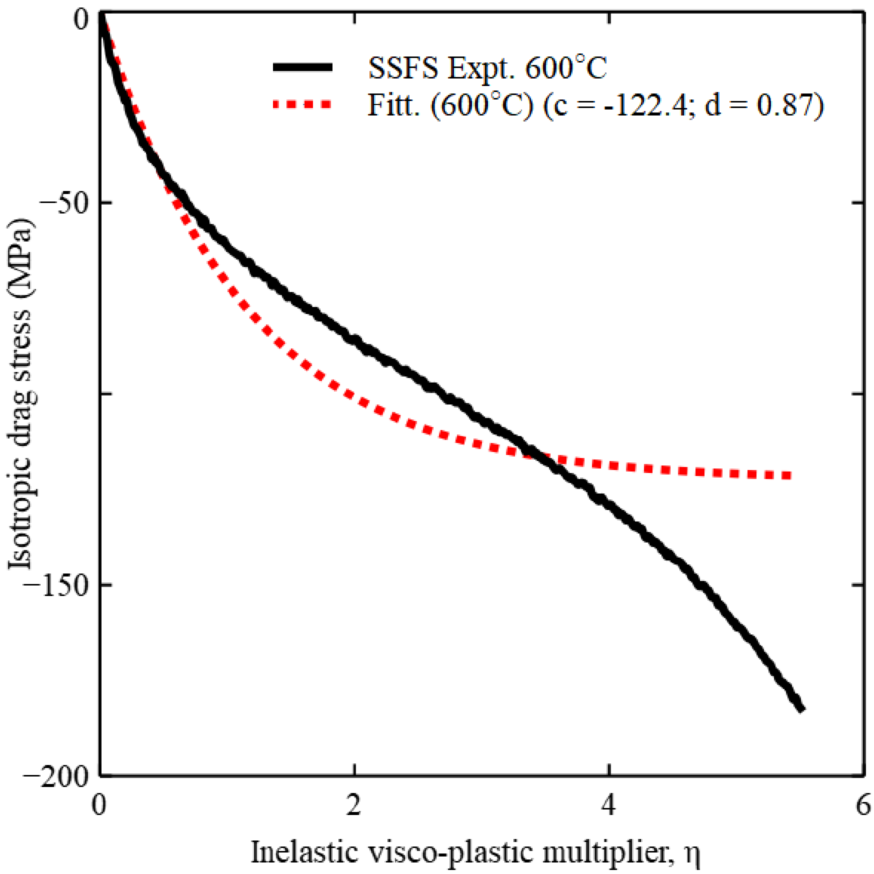

(b)

Figs.5: Comparisons of experimental LCF results for SSFS test with that predicted using the UVP model, (a) Hysteresis loops of the calibrated Chaboche UVP model and cyclic experiment with the first loop, and (b) Comparison of the maximum stress evolution with cycles illustrating softening in FV566 at 600 °C, a strain-range of ± 0.7%, and applied strain-rate of 0.01%s^{-1}.

3.2 Data Correlation

3.2.1 FE Modelling of the non-standard MTP Specimen

Concerning the role of geometry constraint that non-standard MTP specimen has, the complex stress state and the stress triaxiality in essence within the total effective gauge length specimen play an important role in high temperature LCF testing. Thus, it is necessary to evaluate the geometry constraint effect in order to obtain correct transferability between SSFS and non-standard small-sized specimen testing results. To overcome this, the authors have established a new methodology which links the MTP FE model with cyclic UVP constitutive model for determination of scaling factor in order to obtain more accurate applied displacement. The identified scaling factor will be accommodated into high temperature LCF and CF testing of MTP specimen for further comparison and validation.

The identification of scaling factor was simulated through MTP FE model by comparing with SSFS experimental high temperature LCF data. Fig.6a shows an example of non-standard experimental MTP LCF testing set-up. The corresponding 3D FE model, mesh and boundary conditions chosen are given in Fig.6b, while the FE model were performed using C3D8-8 node hexahedral elements. The MTP FE models were constrained in an identical way to the clamping conditions placed on the specimen during LCF testing, as shown in Fig.6a. The extensometers are equivalent to place at the shoulder regions as illustrated in Fig.6b, which is capable to measure the whole deformation including parallel gauge length and transition fillet radius regions.

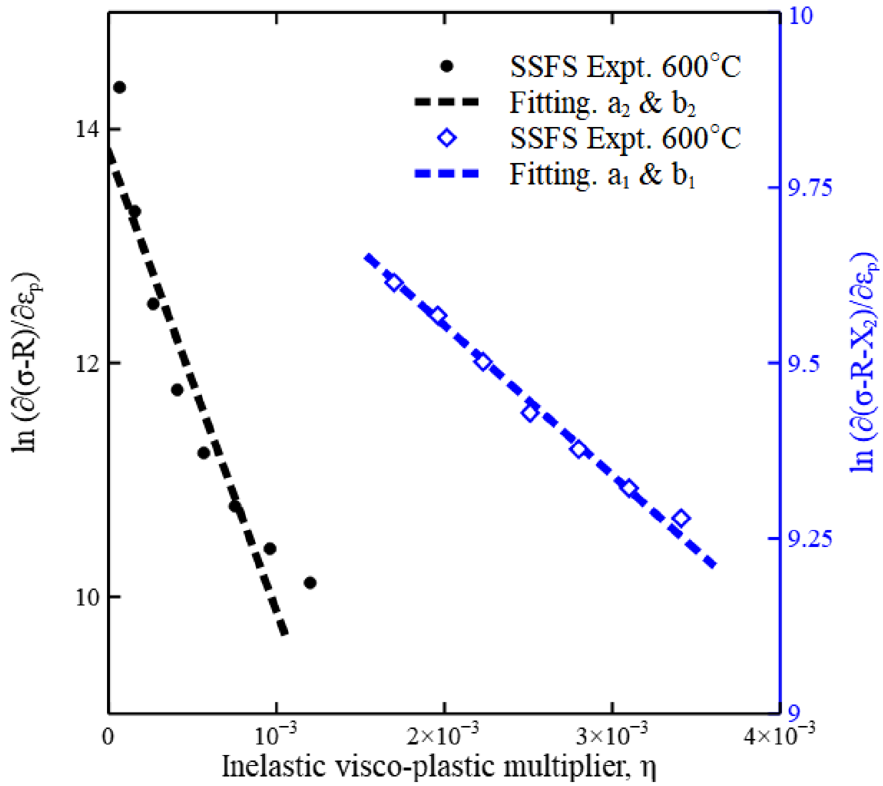

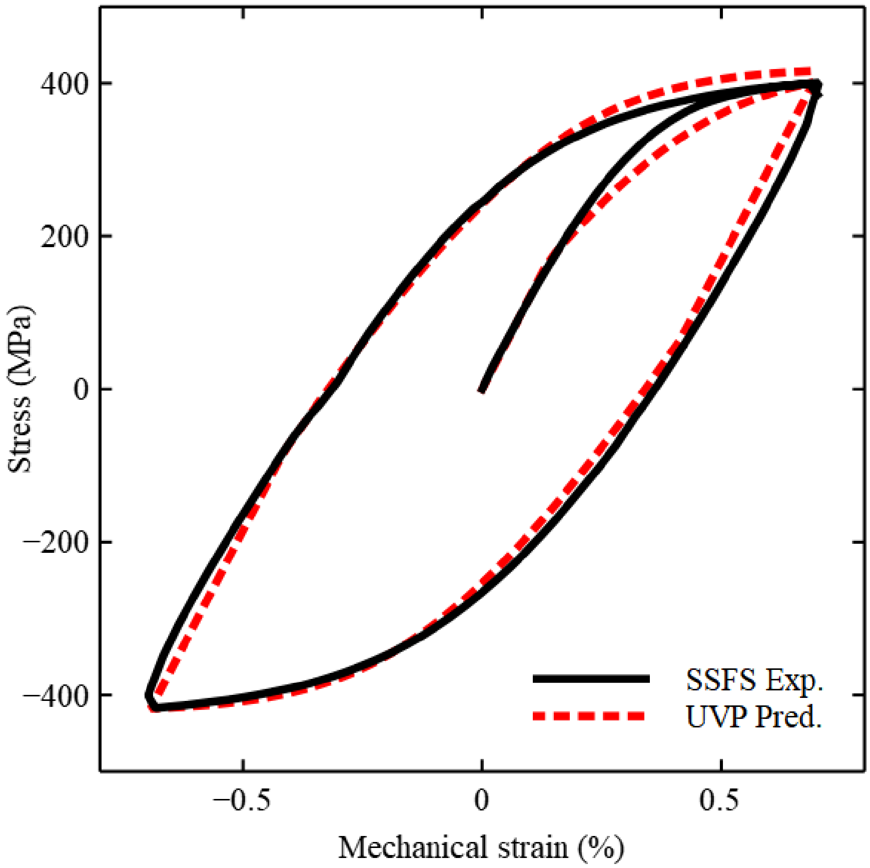

(a) (b)

Figs.6: (a) High temperature LCF and CF tests set-up for MTP specimen, while the total effective gauge length includes the parallel gauge length and the transition fillet radius, and (b) An example of 3D FE model for the proposed MTP specimen including: i) the methodology for scaling factor identification to allow data transferability, and ii) the equivalent locations for placing the extensometer during testing.

Hosted file

`image83.wmf` available at https://authorea.com/users/443699/articles/543644-a-miniaturized-thin-plate-low-cycle-fatigue-test-method-at-elevated-temperature

In order to minimize the accumulated calculation errors and obtain more accurate scaling factor, a prior detailed mesh size effect has been particularly studied and analyzed. All the mesh convergence studies have focused on the parallel gauge length regions to obtain good resolution in terms of average distribution. Four types of mesh strategies are applied with varying mesh sizes from coarser (0.2 mm) to finer (0.05 mm) in the width direction. The results indicate that if the mesh is fine enough, the average responses can be supposed to be almost independent of element size. In the aforementioned numerical simulation, due to computational costs, a fixed element size of ~ 0.1 mm has been chosen for meshing the parallel gauge length area.

3.2.2 Scaling Factor

Hosted file

`image84.wmf` available at https://authorea.com/users/443699/articles/543644-a-miniaturized-thin-plate-low-cycle-fatigue-test-method-at-elevated-temperature

In general, during LCF test for SSFS specimen, the strain deformation can be achieved by the applied displacement dividing the total effective gauge length. However, as can be seen from Fig.6b, it is very difficult to directly calculate the strain deformation since the length between the extensometers consisting of a parallel gauge length and transition fillet radius, thus, a useful deformation correlation between the parallel uniform gauge length (l_0) and transition lengths could not be obtained. In the previous study, the researchers in the work[57] utilized the reference stress approach to allow conventional creep data to be obtained from impression creep test data. Based on the same conception, the authors' have proposed a new reference strain approach for scaling factor identification. On the basis of this, an empirical relationship between the parallel gauge (l_0) and the total effective gauge length () is proposed based on the proposed scaling factor, β , as shown in Fig.6b. The total effective gauge length can be formulated, as follows:

Hosted file

`image85.wmf` available at https://authorea.com/users/443699/articles/543644-a-miniaturized-thin-plate-low-cycle-fatigue-test-method-at-elevated-temperature

(9)

Hosted file

`image86.wmf` available at https://authorea.com/users/443699/articles/543644-a-miniaturized-thin-plate-low-cycle-fatigue-test-method-at-elevated-temperature

The reference average strain, , which is the required mechanical deformation of MTP LCF testing and equal to ± 0.7% in this study, can be calculated through Eq. (10) and Eq. (11), such that:

Hosted file

`image87.wmf` available at https://authorea.com/users/443699/articles/543644-a-miniaturized-thin-plate-low-cycle-fatigue-test-method-at-elevated-temperature

(10)

Hosted file

`image88.wmf` available at https://authorea.com/users/443699/articles/543644-a-miniaturized-thin-plate-low-cycle-fatigue-test-method-at-elevated-temperature

(11)

Hosted file

`image89.wmf` available at https://authorea.com/users/443699/articles/543644-a-miniaturized-thin-plate-low-cycle-fatigue-test-method-at-elevated-temperature

Hosted file

`image90.wmf` available at https://authorea.com/users/443699/articles/543644-a-miniaturized-thin-plate-low-cycle-fatigue-test-method-at-elevated-temperature

in which

is the intended applied displacement on MTP specimen in both FE model and latter high temperature LCF and CF experimental miniature testing, in order to obtain the required strain deformation of ± 0.7% as SSFS LCF test exhibits. is the displacement at the parallel gauge length region. Thus, according to the Eqs. (9) ~ (11), the scaling factor, β , can be formulated, as follows:

Hosted file

`image91.wmf` available at https://authorea.com/users/443699/articles/543644-a-miniaturized-thin-plate-low-cycle-fatigue-test-method-at-elevated-temperature

(12)

Hosted file

`image92.wmf` available at https://authorea.com/users/443699/articles/543644-a-miniaturized-thin-plate-low-cycle-fatigue-test-method-at-elevated-temperature

Therefore, embedding the Eq. (11) into Eq. (12), the displacement,, that applied on the non-standard MTP specimens, can be finally obtained using the following equation:

Hosted file

`image93.wmf` available at https://authorea.com/users/443699/articles/543644-a-miniaturized-thin-plate-low-cycle-fatigue-test-method-at-elevated-temperature

(13)

3.2.3 Determination of the Scaling Factor

A series of numerical simulations were conducted on the non-standard MTP FE models (see Fig.6b), in order to determine the scaling factors. The target of these analysis is to verify whether the MTP model exhibits the identical hysteresis behavior as SSFS specimen when using the correct scaling factors. The material parameters tubulated in Table 1 coupled with the UVP model in Section 3 were accommodated into the MTP FE model. Noted that the hysteresis response of SSFS testing was set as the ultimate target to be achieved by the prediction of MTP FE model via changing the scaling factor with trial and error.

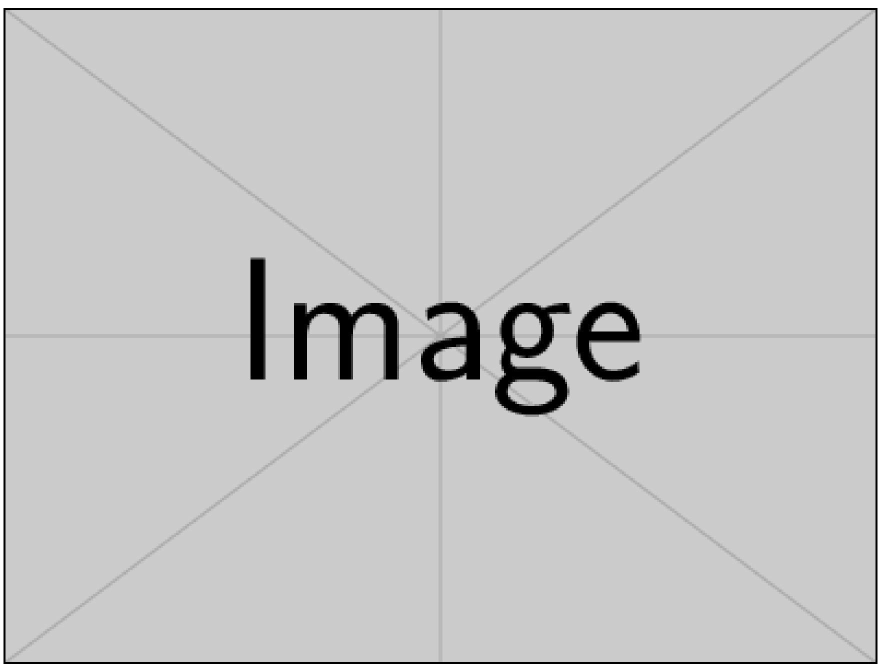

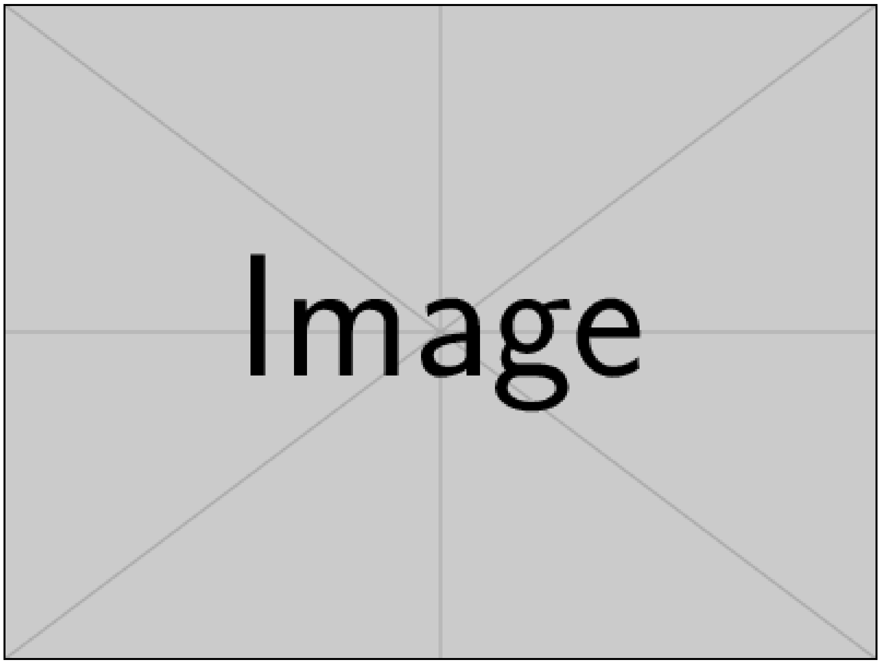

Figs.7 shows the comparisons for the initial cycle between LCF testing result from the SSFS specimen and the predicted results from the MTP FE specimens with varied scaling factors at 600 °C for FV566. The predicted average strain-stress responses in the loading direction, , were extracted from the parallel gauge length regions. Taking the design of $l_0/d_0 = 1.0$ (MTP-1) as an example, it can be observed from Fig.7a that the

hysteresis shape obtained from the numerical FE model changes with the increase of scaling factor (e.g., β increases from 2.0 to 4.0), while the predicted hysteresis curve is in good agreement with SSFS data until β reaches to 4.0. As for the other two MTP samples shown in Figs.7b and 7c, the geometry constraint effect mitigates caused by the increase of l_0/d_0 , leading to an excellent agreement of hysteresis responses with SSFS data using relatively smaller values of scaling factor, for example, $\beta = 3.2$ for MTP-2, and $\beta = 2.7$ for MTP-3, respectively. It can be clearly concluded here that the tentative scaling factors could result in different hysteresis responses for the MTP specimen until an appropriate value occurs. This value is regarded as the finalized scaling factor as tabulated in Table 2, which is capable to provide the excellent predicted hysteresis response and agree well with the experimental SSFS data.

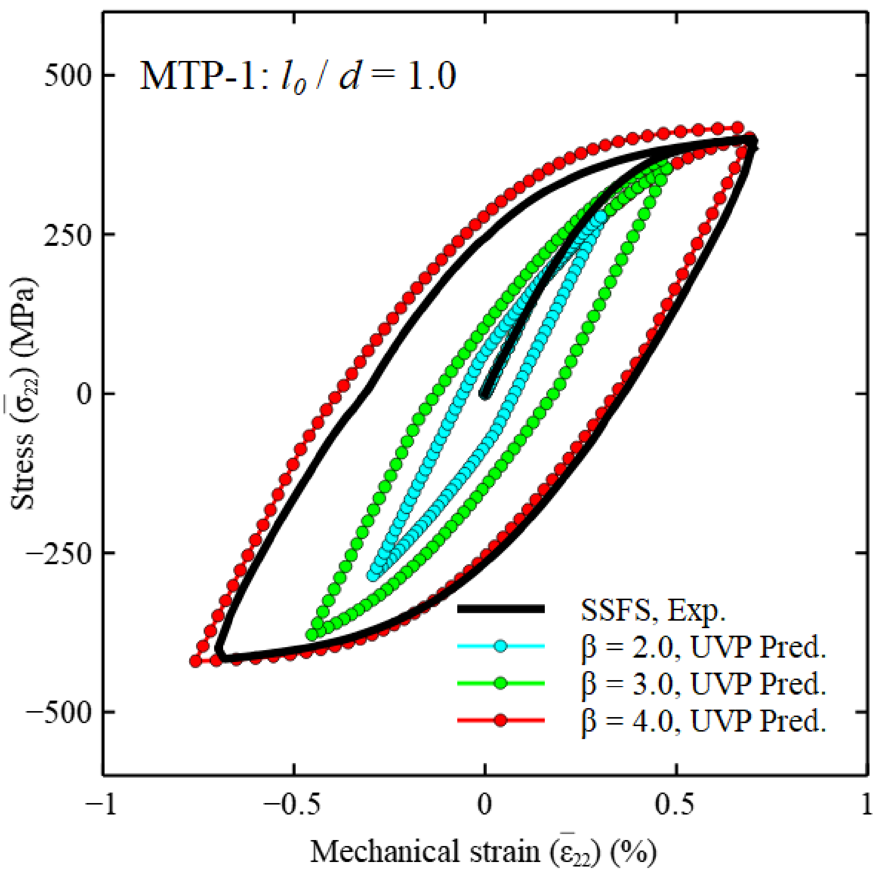

MTP-1: l_0 / d = 1.0
500
250
0
−250
−500
Stress ($\bar{\sigma}_{22}$) (MPa)
−1
−0.5
0
0.5
1
Mechanical strain ($\bar{\varepsilon}_{22}$) (%)
SSFS, Exp.
β = 2.0, UVP Pred.
β = 3.0, UVP Pred.
β = 4.0, UVP Pred.

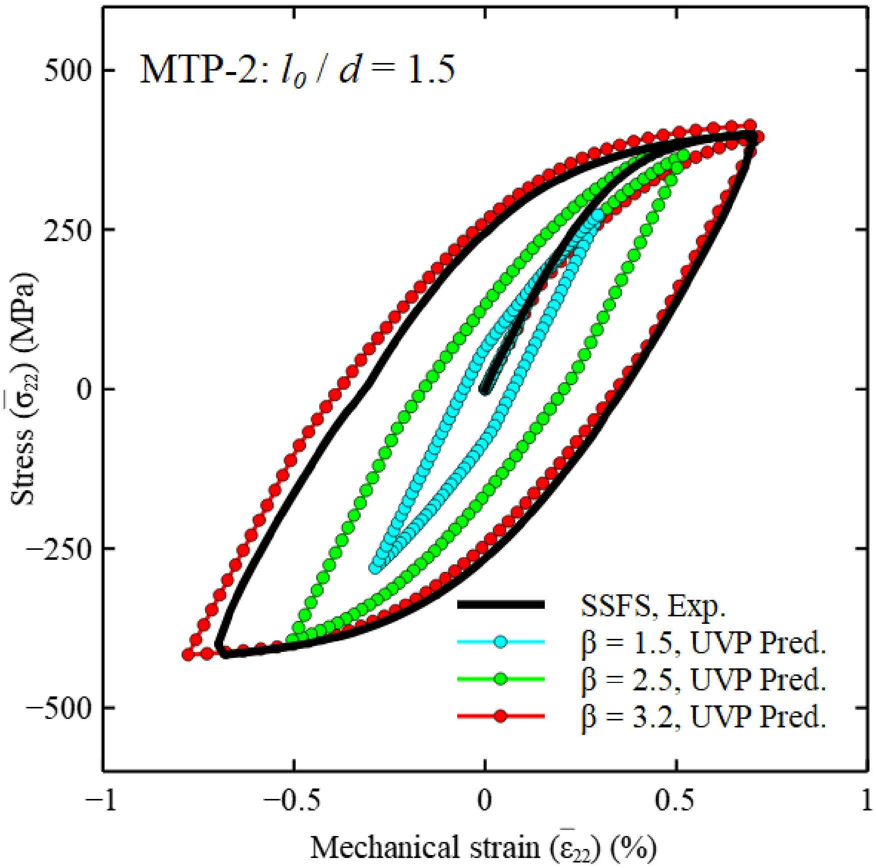

MTP-2: l_0 / d = 1.5
500
250
0
−250
−500
Stress ($\bar{\sigma}_{22}$) (MPa)
−1
−0.5
0
0.5
1
Mechanical strain ($\bar{\varepsilon}_{22}$) (%)
SSFS, Exp.
β = 1.5, UVP Pred.
β = 2.5, UVP Pred.
β = 3.2, UVP Pred.

(b)

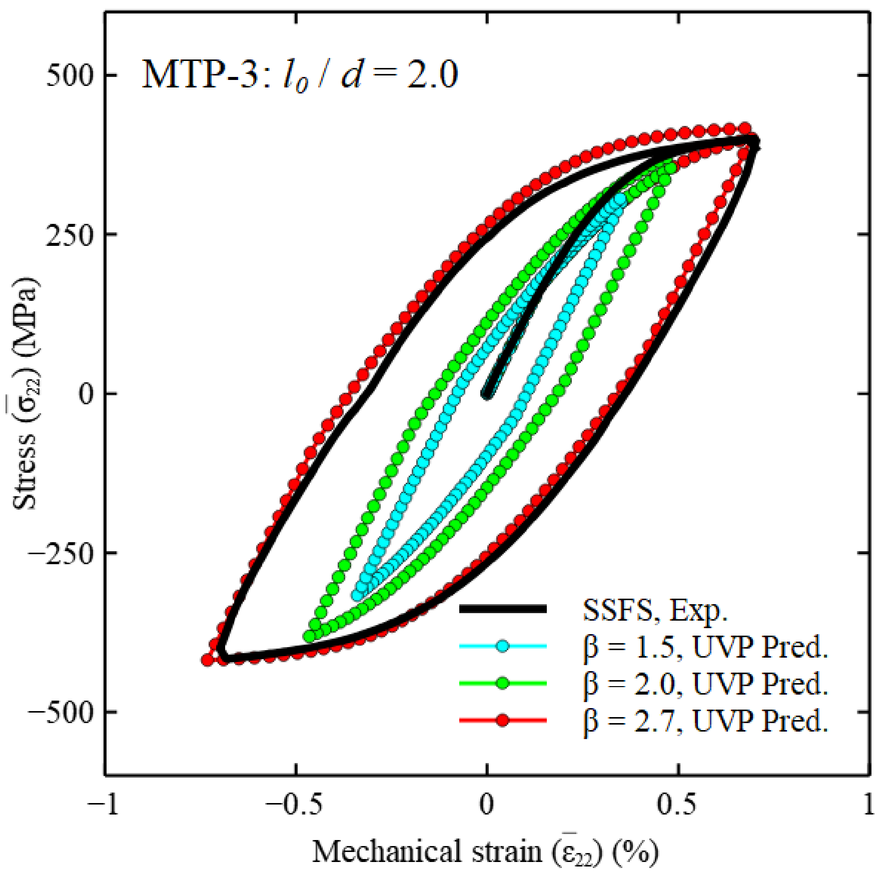

(c)

Figs.7: The comparisons with the initial cycle between SSFS LCF experimental test and UVP predicted hysteresis responses using varied scaling factors based on the proposed 3D FE model introduced in Fig.6b for FV566 at 600 °C. (a)$l_0 / d_0 = 1.0$, (b)$l_0 / d_0 = 1.5$, and (c)$l_0 / d_0 = 2.0$.

Table 2: The values of scaling factor, β , for the MTP specimens based on the UVP model for FV566 steel at 600 .

Specimen	Identified scaling factor, β
MTP-1: l_0/d =1.0	4.0
MTP-2: l_0/d =1.5	3.2
MTP-2: l_0/d =2.0	2.7

To better understand the geometry constraint effect, the predicted dissipated energy that can be determined by calculating the area in the hysteresis loop, A_h , are plotted in Fig.8a. The same principal was also utilized before in the miniature work of Chen*et al.* [58], and Peng *et al* .[34]. As can be seen from Fig.8a, an exponential increase is observed in dissipated energy against scaling factor values. Three exponential equations to determine the scaling factors are fitted and shown in Fig.8a. By using the fitted equations, the scaling factor can be possibly determined for a strain-range deformation required by the MTP high temperature LCF testing under small deformation framework, once the predicted SSFS responses are provided by the UVP model for FV566 at 600 °C. Furthermore, as the increase of scaling factor,β , apparent influence can be observed on the resultant dissipated energy, and this influence is found more pronounced for the finalized scaling factor value in MTP-3. Fig.8b provides the curve in terms of finalized scaling factors versus the ratios ofl_0 $/d_0$. Due to the increase of l_0 $/d_0$, the geometry constraint effect on the finalized identified scaling factors (see Table 2) is obvious, e.g., the geometry constraint effect becomes weaker asl_0 $/d_0$ increases.

Fig.8c shows the computed maximum stress evolution in every cycle until 58$^{\mathrm{th}}$. It is possible to observe that, when the same material properties are accommodated into the MTP FE models for tension and compression testing, the UMAT can gives the inconsistent softening responses due to the geometry constraint effect caused by the changes ofl_0 $/d_{0.}$ A continuous predicted cyclic softening (a decrease in the stress amplitude) can be observed for all MTP specimens, which can be potentially regarded as an implication of accumulated damage and fatigue life[2,17,59,60]. The largest amount of softening with the highest decay-rate can be observed in MTP-1 with the determined,$\beta = 4.0$, due to the strongest geometry constraint effect. The intermediate case can be found in MTP-2, while the amount of softening and decay-rate decelerate in MTP-3. By increasingl_0 $/d_0$ to 2.0, the geometry constraint effect on the decay-rate of softening in MTP-3 has a relatively small impact comparing with MTP-1 and MTP-2.

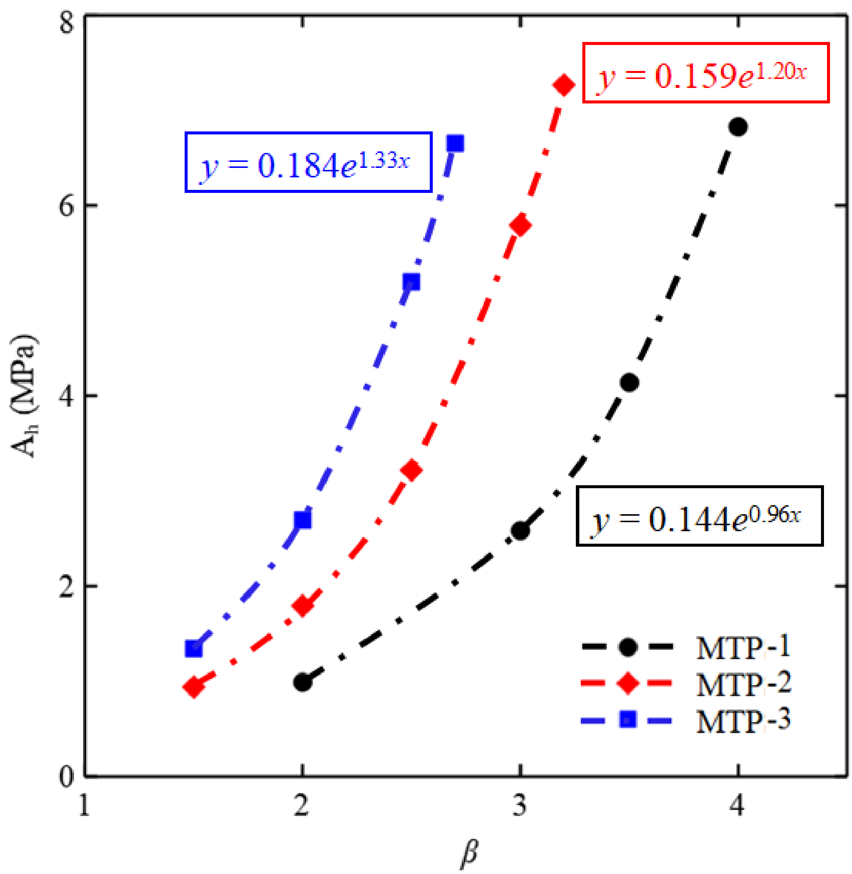

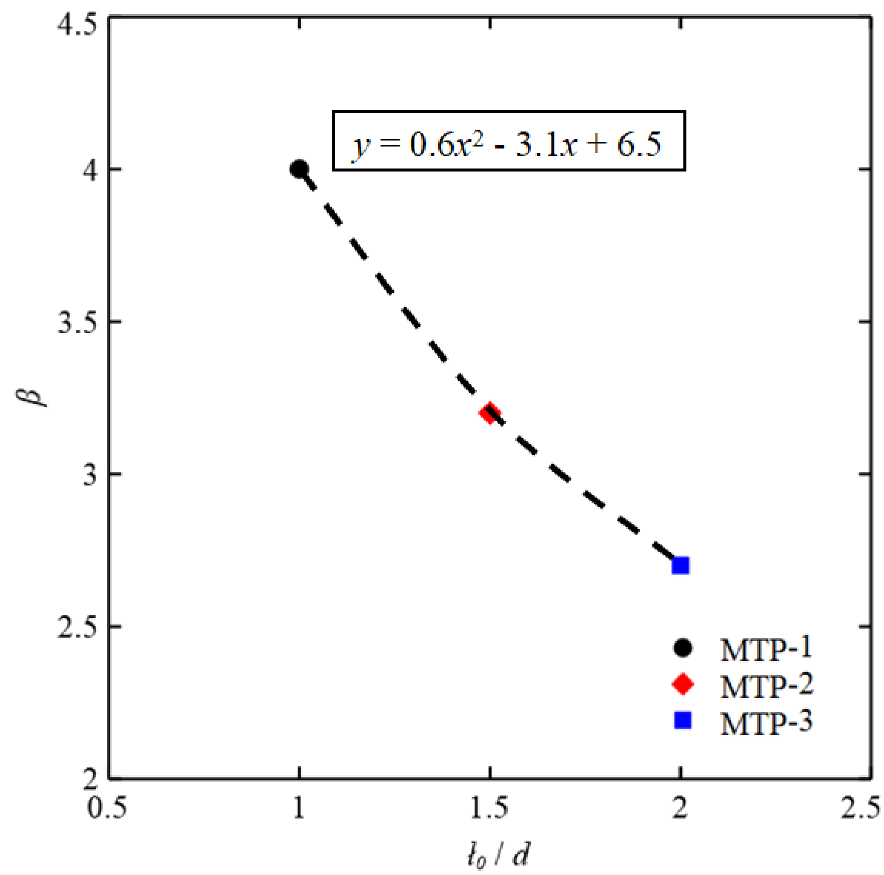

(a) (b)

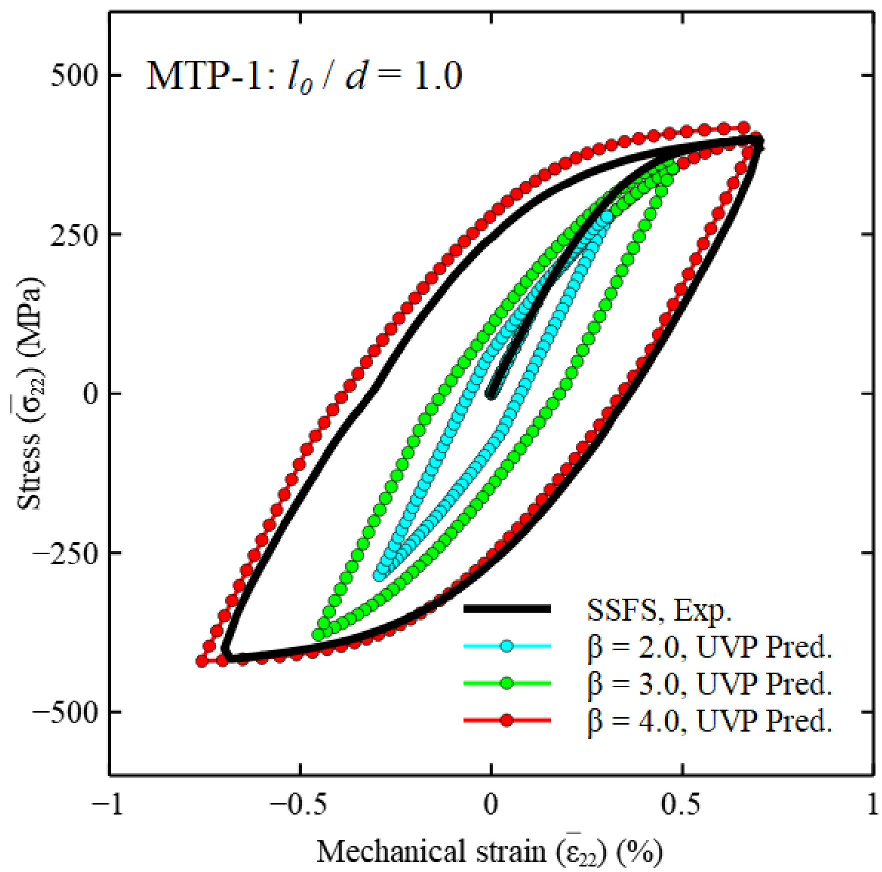

(c)

Figs.8: (a) The fitted curves of the calculated hysteresis area, A_h , for the MTP specimens using different scaling factor values as shown in Fig.7, illustrating obvious geometry constraint effect on hysteresis response; (b) The ultimately determined scaling factor deceases with increasing of l_0 / d_0 for the MTP specimens; and (c) The predicted peak stress evolution using the finalized identified scaling factors for the MTP specimens of FV566 at 600 °C, indicating the geometry constraint effect on cyclic response.

To further examine the mechanical deformation behavior of the three MTP specimens, Figs.9 illustrate the stress and strain distribution under the determined scaling factors (e.g., see Table 2) from loading direction at 600 °C for FV566. Noted that the spatial distribution is extracted from the maximum applied displacement point of the initial cycle at a strain-range of 0.7%. The parallel gauge length regions are marked between the two highlighted lines. In order to make the comparison easier, stress contour plots have been presented using the identical scale. It can be clearly seen from Fig.9a that the highest predicted stress field shows a common uniform pattern at all the parallel gauge length regions, with an approximate average value of ˜ 420 MPa, which is nearly close to the peak stress value that SSFS experimental LCF test exhibits at the same loading point in Fig.7. Additionally, stress heterogeneities can be found at the fillet radius regions due to the non-uniform geometry and unevenly distributed loading. Similarly, strain contours have also been presented in Fig.9b using the same scale for comparison. As can be seen, the highest strain field from loading direction exhibits an average value of ˜ 0.7% between the parallel gauge length, which is the expected mechanical deformation of MTP specimen in this study. Once again, strain heterogeneities can be observed at the fillet radius regions. Thus, according to the numerical perspective in this subsection, it can be confirmed that the proposed reference strain approach coupled with UVP model is capable to identify the correct scaling factor. Furthermore, by using MTP testing, it is possible to obtain consistent high temperature LCF hysteresis deformation as SSFS testing under the equivalent condition, despite the experimental errors and the simplicity of the identification procedure.

Due to the occurrence of geometry constraint effect in non-standard MTP specimen, the multi-axial stress state at the total effective gauge length regions can aggravate the accumulated damage and promote failure such as premature crack initiation under LCF test even a relatively uniform stress-strain pattern is achieved at the initial fatigue cycle. Therefore, it is more useful and necessary to examine the visco-plastic multiplier predicted by the UVP model to see the geometry constraint effect on the subsequent cyclic behavior. Fig.9c presents the predicted visco-plastic multiplier distribution for the three MTP specimens using the determined scaling factors in Table 2 until 58$^{\text{th}}$cycle. Noted that the visco-plastic multiplier contours are set to be with the fixed minimum and maximum scale for a better comparison. As can be seen from Fig.9c, the highest accumulation of plastic strain occurs at the center of MTP-1 specimen with the maximum value of ˜ 0.022%, while MTP-2 is capable to carry less amount of plastic strain with the maximum value of ˜ 0.019% comparing to MTP-1. The accumulation of plastic strain distribution becomes more mitigated with the maximum value of ˜ 0.017% in the case of MTP-3 due to the weakest geometry constraint effect. It can be deduced here that, due to the strongest geometry constraint effect, the plastic strain accumulates at the fastest rate in MTP-1, and consequently leading to the shortest fatigue life in the proposed three non-standard MTP specimens.

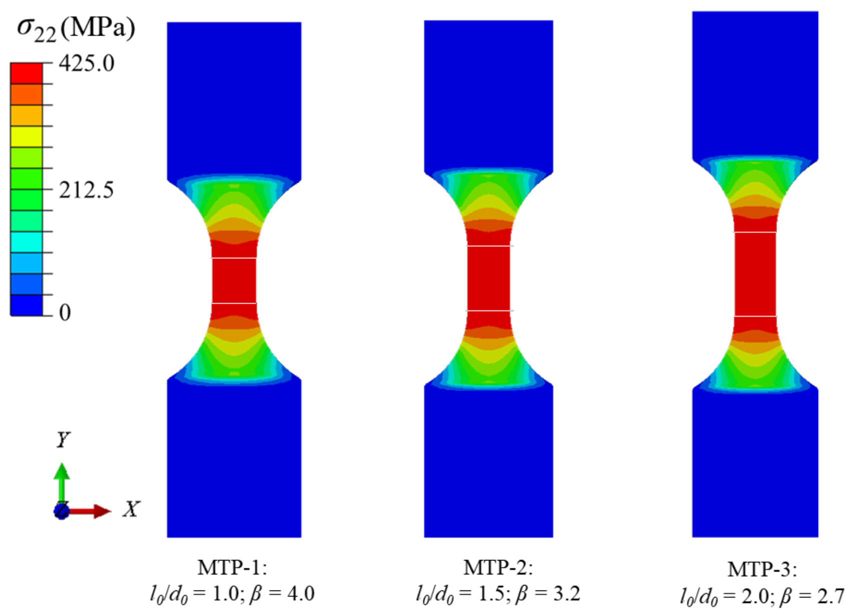

(a)

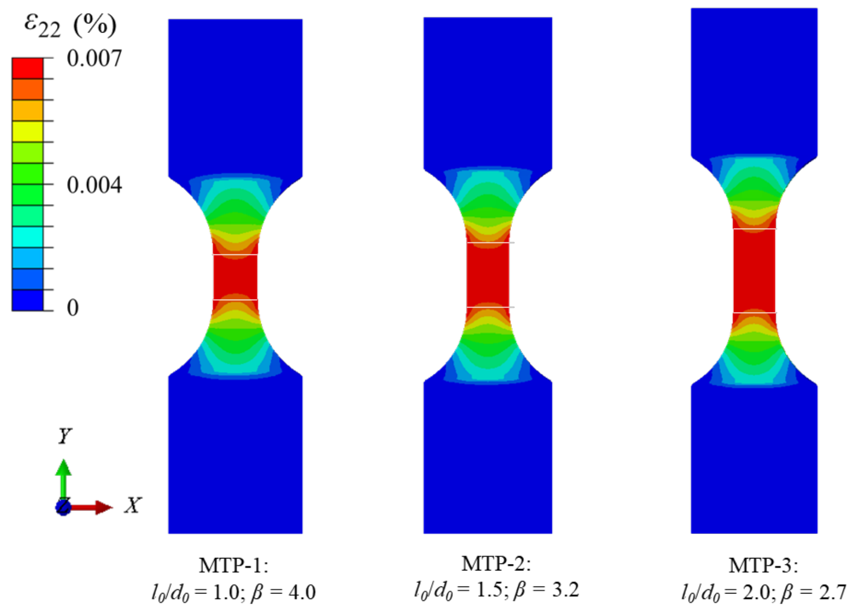

(b)

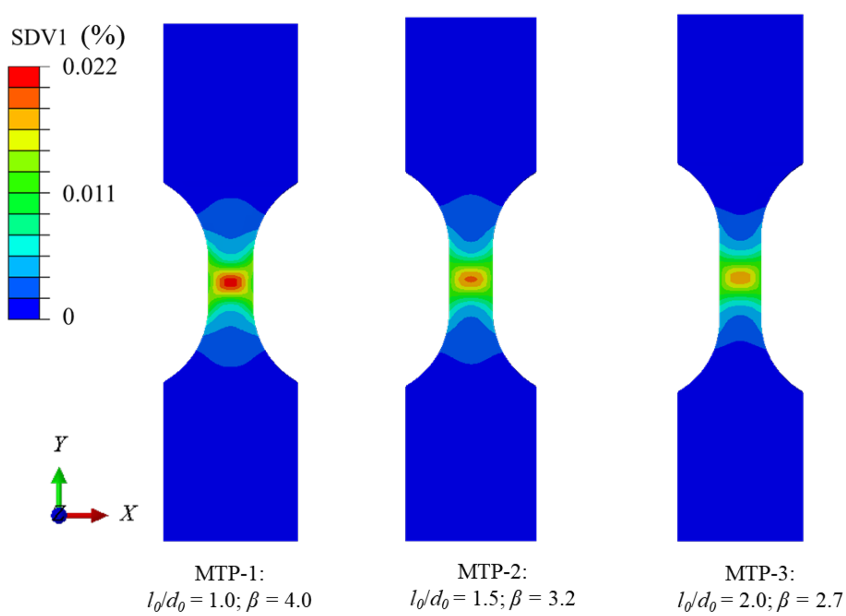

(c)

Figs.9: The predicted spatial distributions of (a) axial stress, (b) axial strain, and (c) visco-plastic multiplier distributions until the 58$^{\text{th}}$ cycle (peak tensile loading point) at the applied strain of 0.7% and strain-rate of 0.01%s^{-1} for the MTP specimens using the ultimately determined scaling factors (Table 2).

From all mentioned in this section, the cyclic elasto-visco-plastic deformation essence of LCF testing for non-standard MTP specimen is the identification of scaling factor using a reliable mechanics-based technique to achieve equivalent high temperature LCF deformation as SSFS specimen exhibits. These simulations have proved that the geometry constraint effect in the MTP specimen is primarily responsible for the finalized identified scaling factor, as well as the subsequent cyclic deformation, which reveals the underlying mechanism of the MTP specimen design principle from the perspective of mechanics. The numerical findings based on UVP model will be checked through experimental LCF test at 600 °C for FV566 in the following sections in order to further demonstrate the testing methodology developed in this study.

4. Experimental Results

4.1 MTP Specimen LCF Saw-Tooth Tests

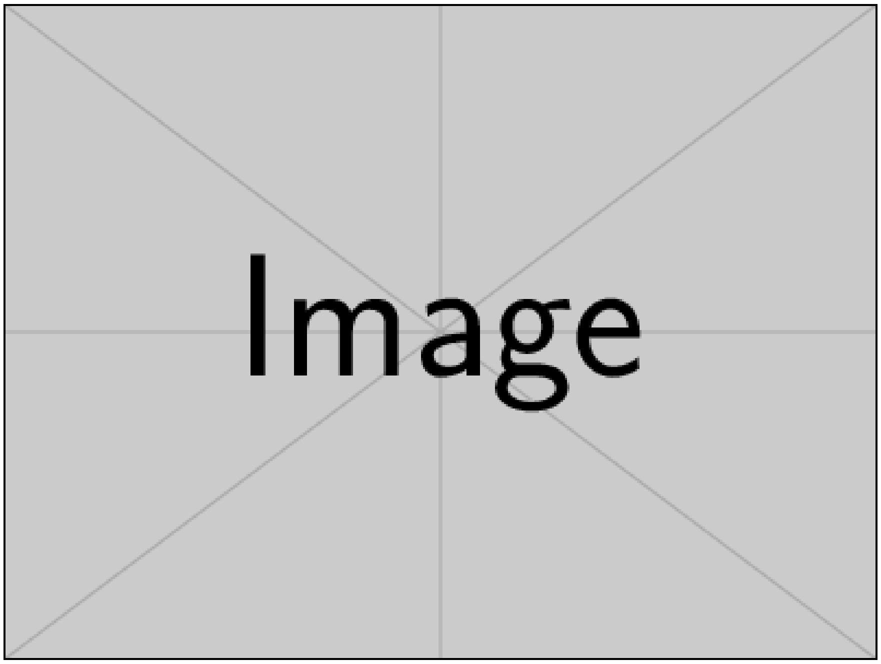

Hosted file

`image103.wmf` available at https://authorea.com/users/443699/articles/543644-a-miniaturized-thin-plate-low-cycle-fatigue-test-method-at-elevated-temperature

Hosted file

`image104.wmf` available at https://authorea.com/users/443699/articles/543644-a-miniaturized-thin-plate-low-cycle-fatigue-test-method-at-elevated-temperature

Figs.10 presents the experimental comparisons of the measured stress-strain hysteresis responses for the 1^{st} cycle between SSFS and MTP specimens for FV566 steel at 600 °C subjected to saw-tooth loading. The accuracy of the 1^{st} hysteresis loop under high temperature LCF test is particularly important as it can be used to determine the elastic and kinematic parameters, e.g.,E , , , , for Chaboche unified visco-plastic model in this paper[1-3]. As can be seen from Fig.10 (left), the reversible hysteresis responses from MTP specimens using the determined scaling factors show an excellent agreement comparing with the SSFS testing results under the equivalent testing conditions, in particularly for the MTP-3 with the weakest geometry constraint effect. In addition, the hysteresis loops of MTP specimens exhibit obvious identical dynamic strain hardening as SSFS testing. To enable a direct comparison of temporal stress evolution behavior between SSFS and MTP specimens, the stress data versus normalized time are plotted in Fig.10 (right), again, showing a very good agreement. Maximum tensile and minimum compressive stresses in the three MTP specimens are nearly identical to those from the SSFS testing for the first cycle, especially for the MTP-3 specimen.

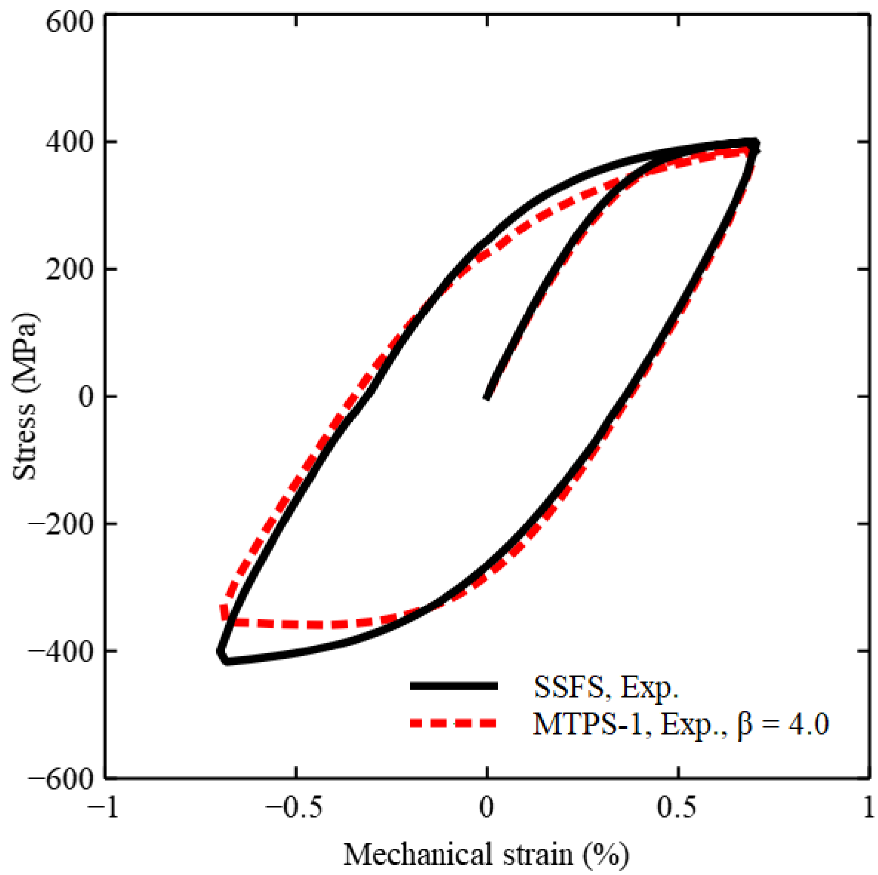

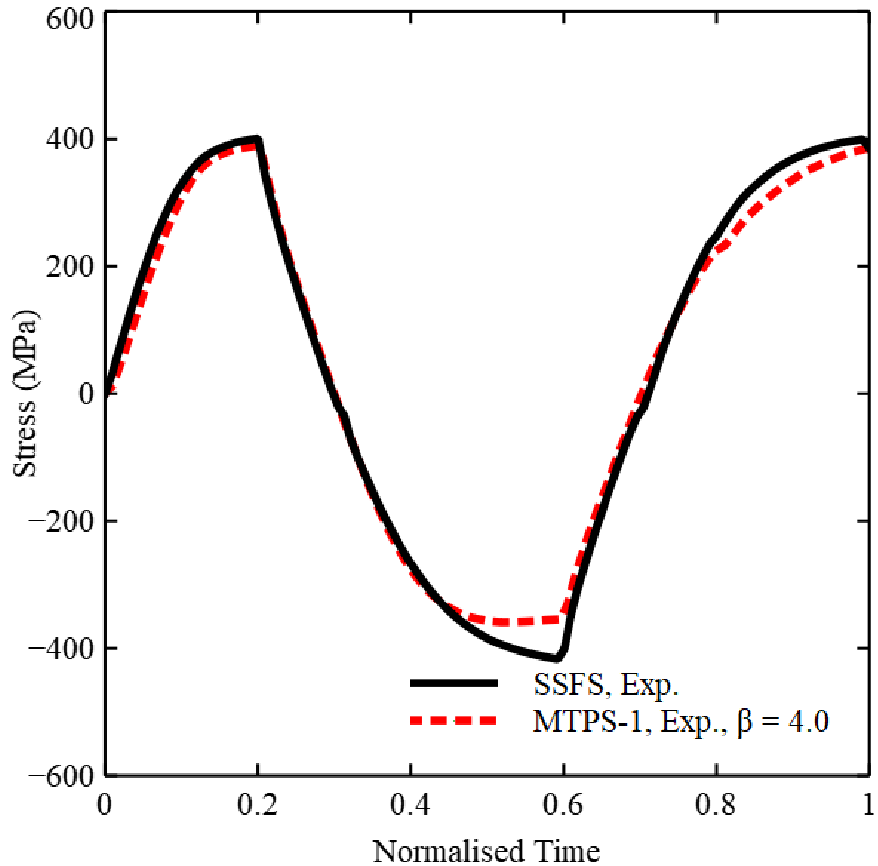

600
400
200
0
−200
−400
−600
Stress (MPa)
0
0.2
0.4
0.6
0.8
1
Normalised Time
SSFS, Exp.
MTPS-1, Exp., β = 4.0

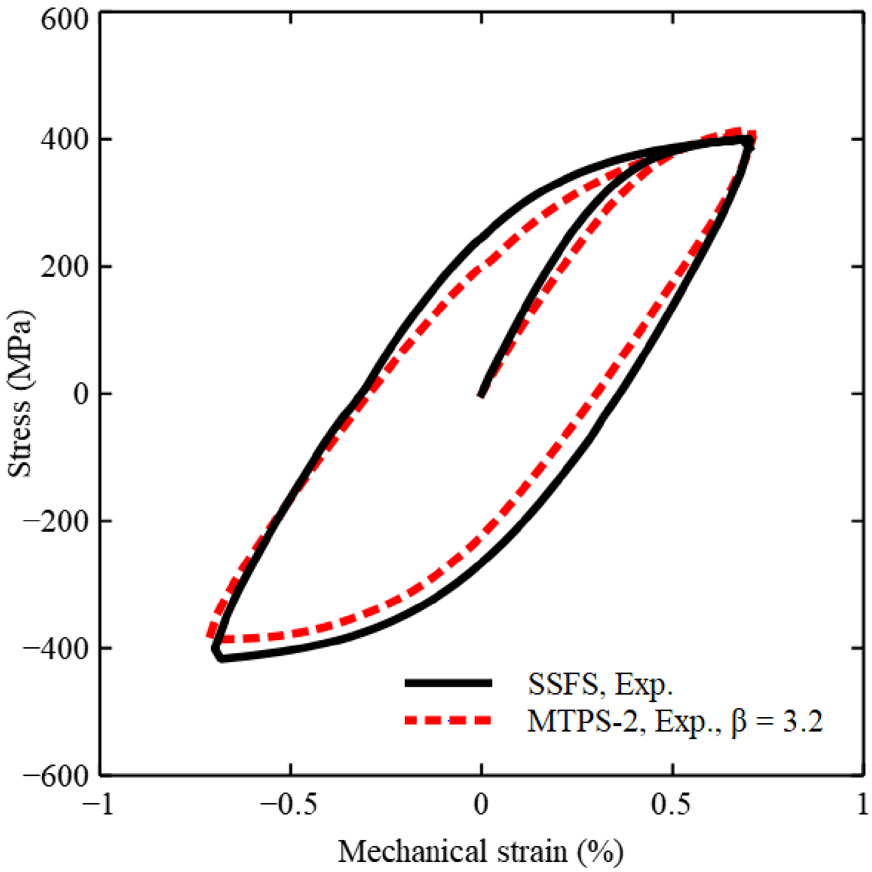
600
400
200
0
−200
−400
−600
Stress (MPa)
−1
−0.5
0
0.5
1
Mechanical strain (%)
SSFS, Exp.
MTPS-2, Exp., β = 3.2

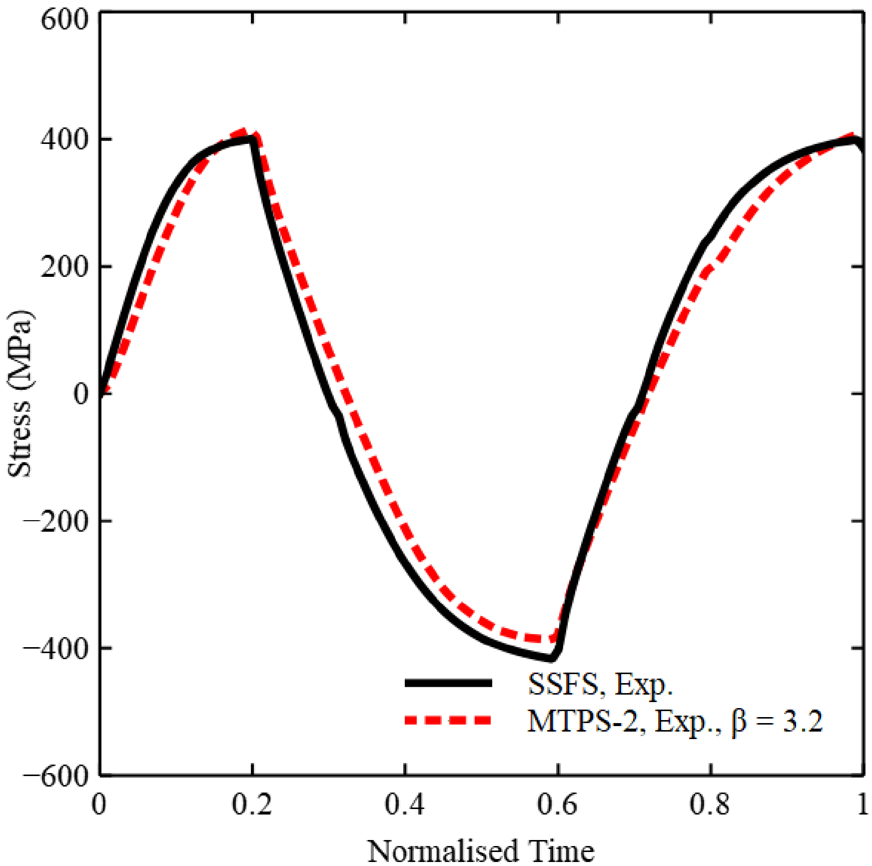

600
400
200
0
−200
−400
−600
Stress (MPa)
0
0.2
0.4
0.6
0.8
1
Normalised Time
SSFS, Exp.
MTPS-2, Exp., β = 3.2

(a) (b)

(c) (d)

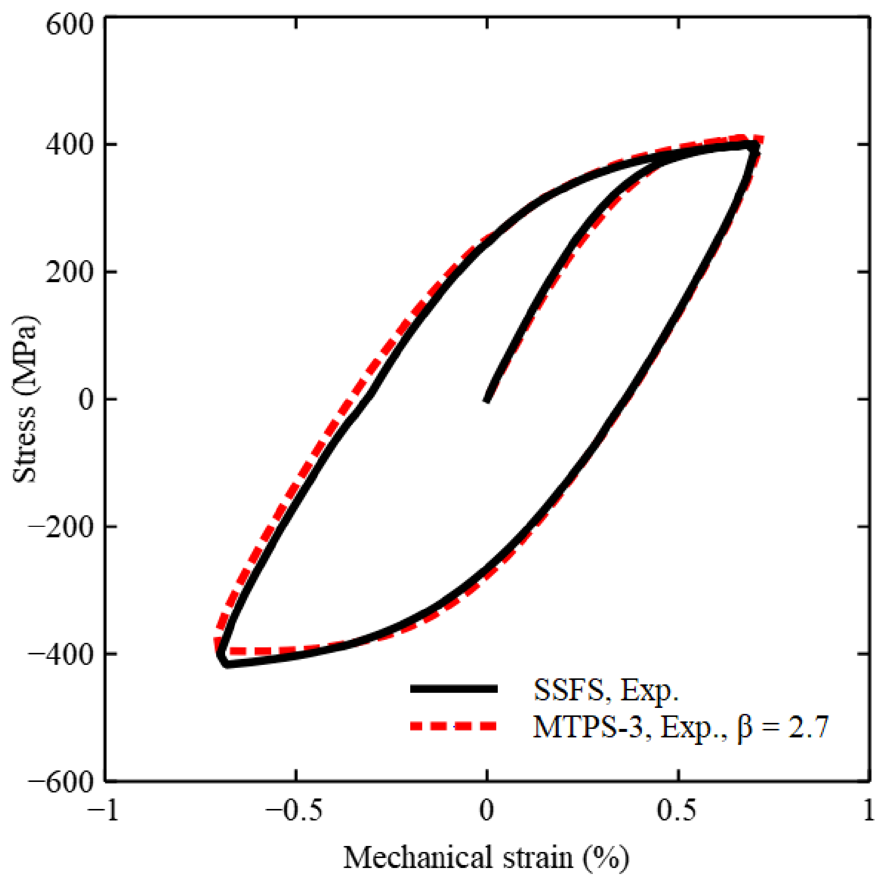

600
400
200
0
−200
−400
−600
Stress (MPa)
−1
−0.5
0
0.5
1
Mechanical strain (%)
SSFS, Exp.
MTPS-3, Exp., β = 2.7

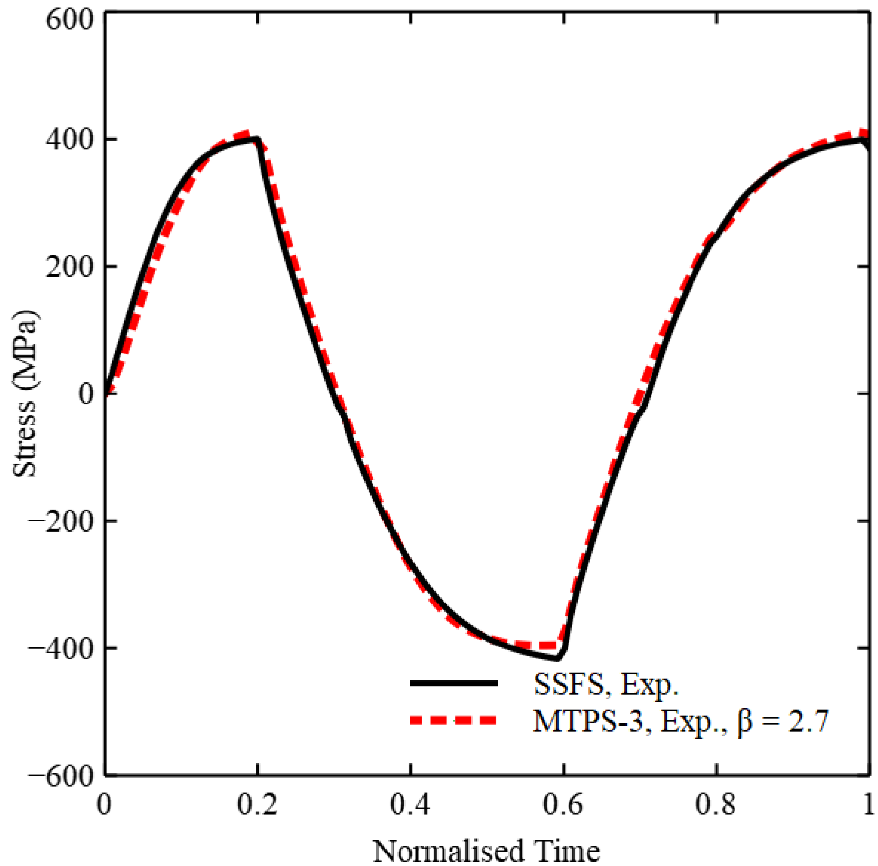

(e) (f)

Figs.10: The comparisons of the tested LCF saw-tooth hysteresis responses for FV566 at 600 °C between SSFS and MTP specimens, (a) and (b) for MTP-1, (c) and (d) for MTP-2, (e) and (f) for MTP-3. The applied strain-rate is 0.01%s^{-1}. The deformation correlation between SSFS and MTP specimen was achieved through the determined scaling factor as shown in Table 2.

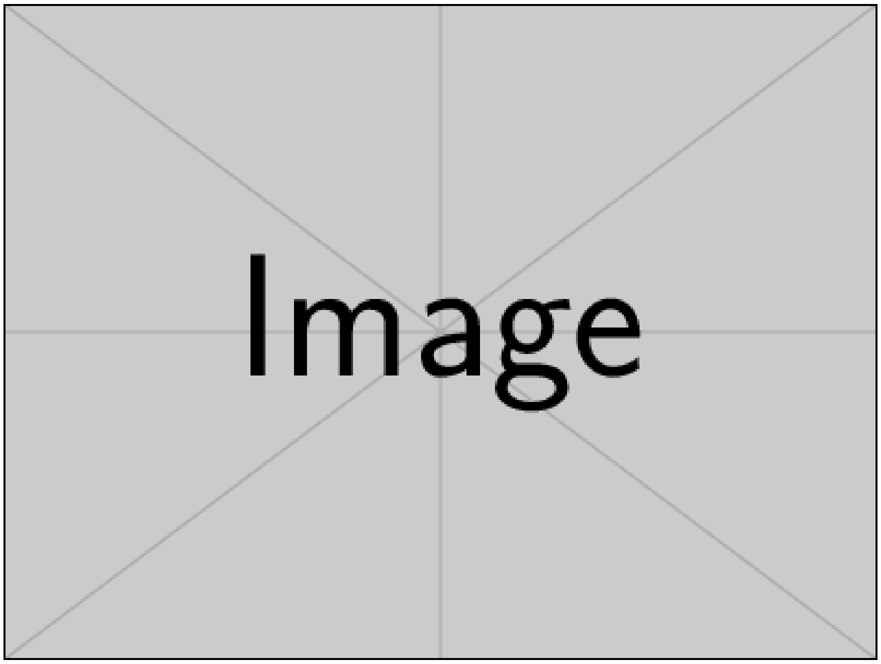

Some of the important experimentally measured parameters are further calculated and compared in Table 3 between the MTP and SSFS specimens, including Young's modulus (E), initial cyclic yield stress (), cyclic strain hardening exponent (n '), together with the cyclic strength coefficient (K ') calculated according to the Ramberg-Osgood relationship[61]. The identified parameters obtained by the MTP-3 specimen can provide excellent agreement with these from SSFS specimen at 600 °C for FV566. Thus, it is concluded that the scaling factors determined from UVP FE method can be used with confidence to correctly covert the measured MTP cyclic deformation data to the same equivalent deformation as SSFS shows in this work. The measured cyclic strain-stress data from MTP LCF test at high temperature can be reliably adopt to evaluate some of the essential parameters required by UVP model[1,3].

Table 3: Comparison of the material parameters based on Ramberg-Osgood relation derived from the SSFS LCF test and the MTP LCF tests for FV566 at 600 .

Specimen	E (MPa)	(MPa)	K' (MPa)	n'
SSFS	120850	168.41	299.6	6.48
MTP-1	120420	166.53	294.3	6.32
MTP-2	118460	154.27	299.8	6.57
MTP-3	120310	167.31	296.5	6.39

4.2 MTP Specimen LCF Dwell Test

The CF dwell tests at high temperature can be used to determine the viscous parameters, i.e., visco-plastic resistance and visco-plastic exponent within Chaboche UVP model, based on the Cottrel's stress partition method[1,3]. As discussed in Section 3.2.3, only CF dwell test using the MTP-3 specimen at 600 °C is carried out and compared with the corresponding SSFS CF dwell test[1], due to the weakest geometry constraint effect. Once again, as can be seen from Fig.11a, the cyclic response of the MTP-3 specimen duplicates very well with the behavior of the SSFS specimen under the equivalent loading conditions. However, a mismatch can be observed in the latter tension-loading stage probably due to slippage between the clamps and specimens. Obvious significant stress relaxation with a dwell period of 2.5hours is observed in the MTP-3 specimen as expected. The corresponding measured stress evolutions versus normalized time for both MTP and SSFS tests at high temperature are presented in Fig.11b. Very small difference of peak stresses can be seen at maximum tension and compression loading points. During the dwell period at the same applied mechanical strain of 0.7%, the stress relaxation in the MTP-3 test is almost the same as that from SSFS test. Satisfactory comparison is obtained for influence of hold time on peak stresses. Thus, the viscous parameters required by UVP model can also be accurately assessed for FV566 steel based on the stress relaxation data from MTP-3 CF testing at high temperature.

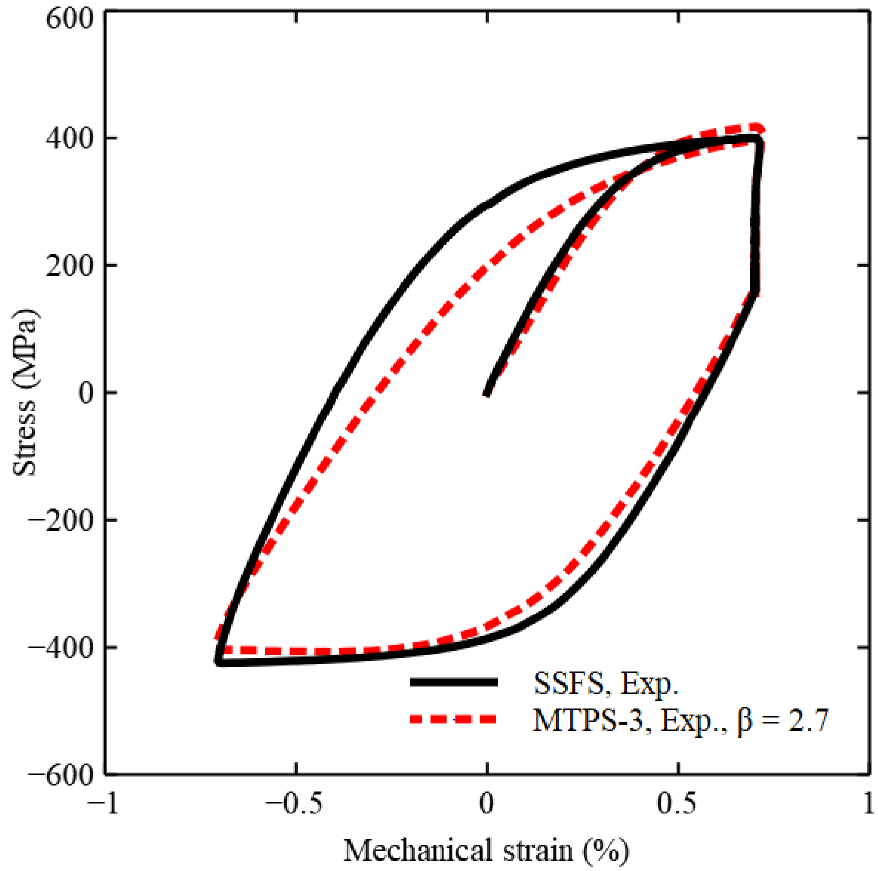

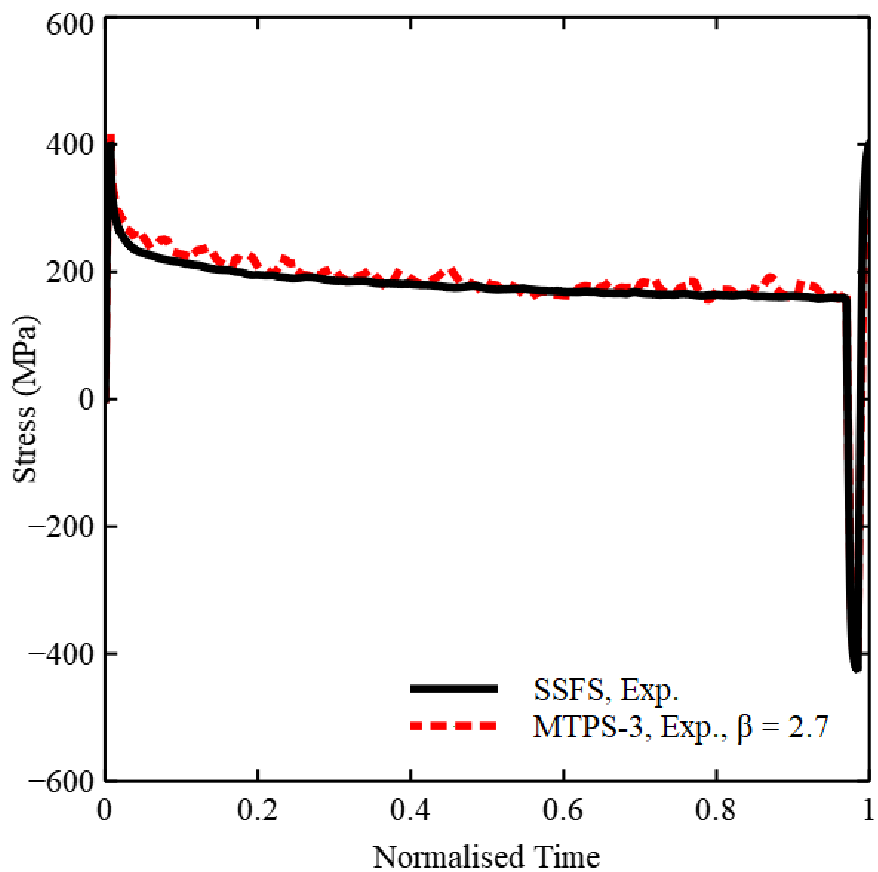

(b)

Figs.11: The comparison of CF dwell-type, (a) hysteresis responses, and (b) Stress evolution versus normalised time at the first cycle obtained from MTP-3 and SSFS specimen tests for FV566 at 600 °C under the applied strain-rate of 0.01%s^{-1}. The hold period is 2.5 hours.

4.3 Cyclic Softening and Fatigue Life

The cyclic softening behavior is also essential for the isotropic parameter identification (c and d in Eq. (8))[1-3,49] in Chaboche UVP model and even damage parameters[62]. Thus, the measured peak stress evolutions versus fatigue lives (N) for both SSFS and MTP tests subjected to saw-tooth and dwell-type loadings are compared in Fig.12. Similar to SSFS fatigue test, significant cyclic softening is observed in MTP specimens with different magnitude levels and rates, as the primary mechanism of cyclic softening in the investigated material is low angle boundary dislocation annihilation[63,64]. In general, the trends of the measured peak stress evolutions in every cycle in the MTP specimens under saw-tooth loading are similar to that of in SSFS specimen. However, cyclic softening and fatigue lives of MTP specimens exhibit a strong geometry dependency. For example, MTP-3 with the weakest geometry constraint effect gives the closest fatigue life comparing with the SSFS test subjected to saw-tooth loading, while MTP-2 is the intermediate case. The shortest fatigue life can be observed in MTP-1 due to the strongest geometry constraint effect. The measured peak stress evolution subjected to saw-tooth waveform in Fig.12 is consistent with the peak stress evolution as predicted in Fig.8c, which further confirm the feasibility of the testing methodology and FE analysis used in this work. The fatigue life of MTP-3 subjected to dwell-type loading is significantly lower than the test under saw-tooth loading because the hold dwell effect can aggravate the damage accumulation, which is consistent with our previous experimental observations on the investigated material[1,3,63,64]. Table 4 tabulates the comparison of fatigue lives (N_f) for all the tests within this test program.

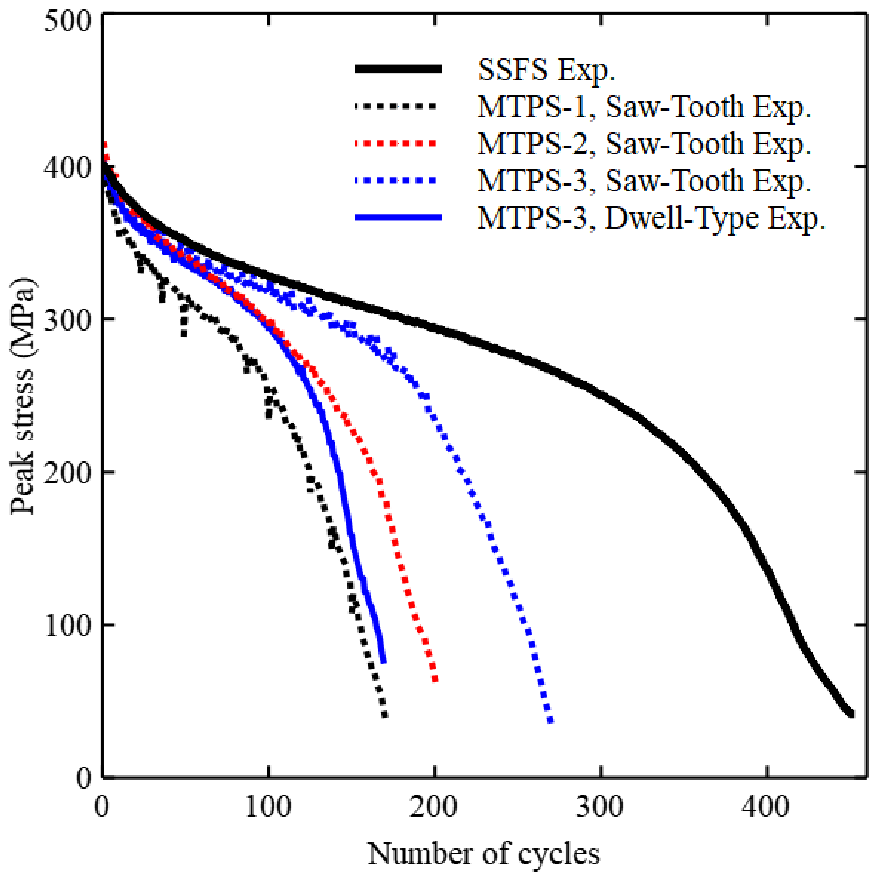

Fig.12: The comparisons of cyclic softening and fatigue life obtained by experimental SSFS and MTP specimen tests for FV566 at 600 °C under the applied strain-range of ± 0.7% and strain-rate of 0.01%s^{-1}.

Table 4: Comparison of the number of cycles to failure, N_f, obtained from the MTP LCF tests and the SSFS LCF test for FV566 at 600 °C.

Specimen Type			Waveform	N_f
SSFS	0.01%s^{-1}	± 0.7%	Saw-Tooth	457
MTP-1				172
MTP-2				200
MTP-3				271
MTP-3			Dwell-Type	170

5. Discussions and Future Work

In this work, a special clamping feature was designed and manufactured, which is capable to produce a rigid displacement transfer and ensure excellent alignment for the MTP specimen in order to minimize the detrimental effects of bending-torsional on the high temperature LCF testing results. To demonstrate the testing technique, good comparisons were achieved regarding the tensile testing between the non-standard MTP and conventional specimens at 20 °C and 600 °C, respectively.

Since the very small-sized specimen used in this work, the uniform uniaxial strain deformation is hard to directly be measured from the parallel gauge length region. Thus, scaling factor, which can be adopt to realize the correct transferability and correlation of LCF testing data between conventional standardized and non-standard MTP specimens, is proposed based on the reference strain approach. The UVP FE model coupled with the identified high temperature LCF material properties for FV566 is employed to determine the scaling factor under the required mechanical deformation. The equivalent energy principal is utilized to evaluate the geometry constraint effect that non-standard MTP specimen has. It was found that the scaling factor is more dependent on the geometry, for example, the ratio ofl_0 /d_0 in this study, which also in turn can be utilized to evaluate the geometry constrain effect.

The feasibility of the non-standard MTP specimen LCF testing technique developed has been further checked via high temperature fully reversed saw-tooth test and CF dwell-type LCF tests for FV566 turbine rotor steel at 600 °C. Good agreement between MTP and SSFS tests is not only achieved for description of the first cycle, but also for the cyclic softening. The experimental results also indicate that fatigue life of MTP specimen is very sensitive to the geometry constraint effect. The thin-plate specimen with lower scaling factor can provide the closest fatigue life comparing with that of SSFS test, for example, MTP-3 saw-tooth test in this work. Additionally, the MTP LCF test results have demonstrated that the methodology developed can be used to represent the high temperature cyclic response of SSFS test, which can be further adopt to identify the elastic, kinematic and viscous parameters required by Chaboche type high temperature UVP model.

High temperature LCF testing approach for MTP specimen have been discussed in this work, but many issues remaining are still required to be sorted out with more experimental testing. For example, the reasons for lower fatigue life in the MTP specimen are not apparent. Further investigations should be carried out to continuously improve the testing rigs, such as the new design for the clamp fixtures to reduce slippage, new design of MTP specimen with higher ratio ofl_0 /d_0 to more accurately capture the total fatigue life of SSFS specimen and obtain more accurate isotropic parameters at high temperature. The surface roughness conditions are particularly critical for the MTP specimen because the effect of surface finishing on miniature LCF life is expected to be more significant than on SSFS specimen. Moreover, more metallographic investigations are needed to identify the cause of the failure mechanism and to improve results at high temperature as well. For example, MTP specimen at high temperature is prone to have oxidation damage, leading to premature fatigue crack initiation and the reduction of fatigue life. Although the possible trends for the size effect have been introduced in the refs[65,66], available data are still rather scare, especially for size effect at high temperature. More investigation should be carried out in this scope as well in the future.

Author Statement Contribution

Ming Li : Conceptualization, Methodology, Software, Formal analysis, Investigation, Data curation, Writing – original draft.**Shane Maskill** : Experiments. Zhixun Wen: Review & editing.**Zhufeng Yue** : Writing – review & editing, Supervision, Project administration, Funding acquisition. **Wei Sun** : Conceptualization, Methodology, Writing – review & editing, Supervision, Project administration, Funding acquisition.

Acknowledgment

This work is supported by the Engineering and Physical Sciences Research Council UK (grant number: EP/N509991/1). This research was also supported by the National Natural Science Foundation of China (grant number: 51875461).

References:

1. Rae, Y., Benaarbia, A., Hughes, J., Sun, W., Experimental characterisation and computational modelling of cyclic viscoplastic behaviour of turbine steel. *International Journal of Fatigue* , 2019; **124** : p. 581-594.
2. Li, M., Barrett, A. R., Scully, S., Harrison, M.N., Leen, S.B., O'Donoghue, P.E., Cyclic plasticity of welded P91 material for simple and complex power plant connections. *International Journal of Fatigue*

, 2016; **87** : p. 391-404.

3. Li, M., Benaarbia, A., Morris, A., Sun, W., Assessment of potential service-life performance for MarBN steel power plant header under flexible thermomechanical operations. *International Journal of Fatigue* , 2020; **135** : 105565.
4. Rhys-Jones, T.N., and Cunningham, T.P., The influence of surface coatings on the fatigue behaviour of aero engine materials.*Surface and Coatings Technology* , 1990; **42** (1): p. 13-19.
5. Hyde, T.H., and Sun, W., A novel, high-sensitivity, small specimen creep test. *Journal of Strain Analysis for Engineering Design* , 2009; **44** (3): p. 171-185.
6. Chen, H., Jackson, G.A., and Sun, W., An overview of using small punch testing for mechanical characterization of MCrAlY bond coats.*Journal of Thermal Spray Technology* , 2017; **26** (6): p. 1222-1238.
7. Chen, H., and Hyde, T.H., Use of multi-step loading small punch test to investigate the ductile-to brittle transition behaviour of a thermally sprayed CoNiCrAlY coating. *Materials Science and Engineering A* , 2017; **680** : p. 203-209.
8. Hyde, T. H., Sun W., and Williams, J. A., The requirements for and the use of miniature test specimens to provide mechanical and creep properties of materials: - a review. *International Materials Reviews* , 2007; **52** (4), 213-255.
9. Hyde, T.H., Hyde, C.J., and Sun, W., Theoretical basis and practical aspects of small specimen creep testing. *Journal of Strain Analysis for Engineering Design* , 2013; **48** (2): p. 112-125.
10. Hyde, T.H., Hyde, C.J., and Sun, W., A basis for selecting the most appropriate small specimen creep test type. *Journal of Pressure Vessel Technology-Transactions of the Asme* , 2014;**136** (2): p. 024502-1-024502-6.
11. Morris, A., Cacciapuoti, B., and Sun, W., The role of small specimen creep testing within a life assessment framework for high temperature power plant. *International Materials Reviews* , 2018;**63** (2): p. 102-137.
12. Wen, W., Becker, A.A., and Sun, W., Determination of material properties of thin films and coatings using indentation tests: a review. *Journal of Materials Science* , 2017;**52** (21): p. 12553-12573.
13. Wen, W., Sun, W., and Becker, A.A., A two-material miniature specimen test method and the associated inverse approach for high temperature applications. *Theoretical and Applied Fracture Mechanics* , 2019; **99** : p. 1-8.
14. Xu, X., Benaarbia, A., Allena, D.J., Jepsona, M.A.E., Sun, W., Investigation of microstructural evolution and creep rupture behaviour of 9% Cr MarBN steel welds. *Materials Science and Engineering A* , 2020; **791** : 139546.
15. Dyson, C. C., Sun, W., Hyde, C. J., Brett, S. J., and Hyde, T. H., Use of small specimen creep data in component life management: a review. *Materials Science and Technology* , 2016;**32** (15): p. 1567-1581.
16. Hyde, T. H., Sun, W., Becker, A. A., Williams, J. A., Creep properties and failure assessment of new and fully repaired P91 pipe welds at 923 K. *Proceedings of the Institution of Mechanical Engineers Part L-Journal of Materials-Design and Applications* , 2004;**218** (L3): p. 211-222.
17. Li, M., Sun, F. W., Li, D. F., O'Donoghue, P. E., O'Dowd, N. P., Leen, S. B., The effect of ferrite phases on the micromechanical response and crack initiation in the inter-critical heat-affected zone of a welded 9Cr martensitic steel, *Fatigue & Fracture of Engineering Materials & Structures* , 2018; **41** : p. 1245-1259.
18. Gussev, M. N., Howard, R. H., Terrani, K. A. T., Field, K. G., Sub-size tensile specimen design for in-reactor irradiation and post-irradiation testing. *Nuclear Engineering and Design* , 2017;**320** : p. 298-308.
19. Sastry, D.H., Impression creep technique - An overview.*Materials Science and Engineering* A, 2005; **409** (1-2): p. 67-75.
20. Hyde, T.H., Sun, W., and Becker, A.A., Analysis of the impression creep test method using a rectangular indenter for determining the creep properties in welds. *International Journal of Mechanical Sciences* , 1996; **38** (10): p. 1089-1102.
21. Kumar, S., Ramteke, S., Chelik, S., Vanitha, C., Creep behavior of Al-Si-Mg alloy by hot impression

creep test. *Materials Today-Proceedings* , 2021; **41** : p. 1207-1211.

22. Dobeš, F. and Milička, K., On the Monkman–Grant relation for small punch test data. *Materials Science and Engineering: A* , 2002; **336** (1-2): p. 245-248.
23. Bruchhausen, M., Holmström, S., Simonovski, I., Austin, T., Lapetite, J.-M., Ripplinger, S., Haan, F., Recent developments in small punch testing: Tensile properties and DBTT. *Theoretical and Applied Fracture Mechanics* , 2016; **86** : p. 2-10.
24. Simonovski, I., Holmstrom, S., and Bruchhausen, M., Small punch tensile testing of curved specimens: Finite element analysis and experiment. *International Journal of Mechanical Sciences* , 2017; **120** : p. 204-213.
25. Jackson, G.A., Bai, M., Pala, Z., Hussain, T., Sun, W., Small punch creep testing of thermally sprayed Stellite 6 coating: A comparative study of as-received vs post-heat treatment. *Materials Science and Engineering A* , 2019; **749** : p. 137-147.
26. Jackson, G.A., Sun, W., and McCartney, D.G., The influence of microstructure on the ductile to brittle transition and fracture behaviour of HVOF NiCoCrAlY coatings determined via small punch tensile testing. *Materials Science and Engineering A* , 2019;**754** : p. 479-490.
27. Cuesta, I.I., and Alegre, J.M., Determination of the fracture toughness by applying a structural integrity approach to pre-cracked small punch test specimens. *Engineering Fracture Mechanics* , 2011; **78** (2): p. 289-300.
28. Yu, H.Y., Zhou, G.Y., Tu, S.T., Zhang, F.K., A new approach to evaluate material creep properties by C-shape ring specimen with fixed constraints. *International Journal of Pressure Vessels and Piping* , 2021; **191** : 104357.
29. Hyde, T.H., Sun, W., Nardone, S., De Bruycker, E., Small ring testing of a creep resistant material. *Materials Science and Engineering A* , 2013; **586** : p. 358-366.
30. Hyde, T.H., Ali, B.S.M., and Sun, W., Analysis and design of a small, two-bar creep test specimen. *Journal of Engineering Materials and Technology-Transactions of the ASME* , 2013; **135** (4): p. 041006-1-041006-9.
31. Wen, W., Jackson, G.A., Li, H., Sun, W., An experimental and numerical study of a CoNiCrAlY coating using miniature specimen testing techniques. *International Journal of Mechanical Sciences* , 2019;**157** : p. 348-356.
32. Cortellino, F., Rouse, J.P., Cacciapuoti, B., Sun, W., and Hyde, T. H., Experimental and numerical analysis of initial plasticity in P91 steel small punch creep samples. *Exp Mech.* , 2017;**57** (8): p.1193-1212.
33. Wen, W., Jin, X.Z, Liu, H., Sun, W., Determination of creep damage properties from small punch creep tests considering pre-straining effect using an inverse approach. *Mechanics of Materials* , 2019;**139** : 103171.
34. Peng, Y.Q., Cai, L.X., Chen, H., Bao, C., A new method based on energy principle to predict uniaxial stress–strain relations of ductile materials by small punch testing, *International Journal of Mechanical Sciences* , 2018; **138-139** : p. 244-249.
35. Li, Y.Z., Stevens, P., Sun, M.C., Zhang, C.Q., Wang, W., Improvement of predicting mechanical properties from spherical indentation test,*International Journal of Mechanical Sciences* , 2016;**117** : p. 182-196.
36. Wang, H., Wang, Q.D., Boehlert, C.J., Yang, J., Yin, D.D., Yuan, J., Ding, W.J., The impression creep behavior and microstructure evolution of cast and cast-then-extruded Mg-10Gd-3Y-0.5Zr, *Materials Science and Engineering: A* , 2016; **649** : p. 313-324.
37. Sakthivel, T., Sasikala, G., Vasudevan, M., Role of microstructures on heterogeneous creep behaviour across P91 steel weld joint assessed by impression creep testing, *Materials Characterization* , 2020;**159** , 109988.
38. Zhuang, F.K., Tu, S.T., Zhou, G.Y., Wang, Q.Q., Assessment of creep constitutive properties from three-point bending creep test with miniaturized specimens. *Journal of Strain Analysis for Engineering Design* , 2014; **49** (7): p. 482-491.
39. Yang, S.S., Cao, Y., Ling, X., Qian, Y., Assessment of mechanical properties of Incoloy800H by means

of small punch test and inverse analysis. *Journal of Alloys and Compounds* , 2017; **695** : p. 2499-2505.

40. J., Džugan, R., Procházka, P., Konopík, Sokolov, M.A., Lucon (Eds.), E., Small Specimen Test Techniques, 6$^{\text{th}}$ Volume,*ASTM International* , New York, 2015; p. 12–29.
41. J. Džugan, P., Konopik, M., Rund, R., Prochazka, Determination of Local Tensile and Fatigue Properties with the Use of Sub-Sized Specimens, *ASME conference* , Boston, 2015.
42. J., Džugan, R., Procházka, P., Konopík, Low Cycle Fatigue Tests with the Use of Miniaturized Test Specimens, *ASME conference* , Hawai, 2017.
43. Lancaster, R.J., Illsley, H.W., Hurst, R., Jeffs, S., Baxter, G., A novel approach to small punch fatigue testing. *Key Engineering Materials* , 2017; **734** : p. 61-69.
44. Lancaster, R.J., Jeffs, S.P., Illsley, H.W., Argyrakis, C., Hurst, R.C., Baxter, G.J., Development of a novel methodology to study fatigue properties using the small punch test. *Materials Science and Engineering A* , 2019; **748** : p. 21-29.
45. Nozaki, M., Sakane, M., and Fujiwara, M., Low cycle fatigue testing using miniature specimens. *International Journal of Fatigue* , 2020; **137** : 105636.
46. Nogami, S., Hasegawa, A., and Yamazaki, M., Fatigue properties of ferritic/martensitic steel after neutron irradiation and helium implantation. *Nuclear Materials and Energy* , 2020; **24** : 100764.
47. Pahlavanyali, S., Rayment, A., Roebuck, B., Drew, G., Rae, C.M.F., Thermo-mechanical fatigue testing of superalloys using miniature specimens. *International Journal of Fatigue* , 2008;**30** (2): p. 397-403.
48. Turnbull, A. and Zhou, S., Comparative evaluation of environment induced cracking of conventional and advanced steam turbine blade steels. Part 1: Stress corrosion cracking. *Corrosion Science* , 2010; **52** (9): p. 2936-2944.
49. Benaarbia, A., Rae, Y., and Sun, W., Unified viscoplasticity modelling and its application to fatigue-creep behaviour of gas turbine rotor.*International Journal of Mechanical Sciences* , 2018; 136: p. 36-49.
50. Dai, C.Y., Zhang, B., Xu, J., Zhan, G. P., On size effects on fatigue properties of metal foils at micrometer scales, *Material Science and Engineering: A* , 2013; **575** , p. 217-222.
51. Kohno, Y., Kohyama, A., Hamilton, M.L., Hirose, T., Katoh, Y., Garner, F.A., Specimen size effects on the tensile properties of JPCA and JFMS. *Journal of Nuclear Materials* , 2000; **283** : p. 1014-1017.
52. Howard, C., Frazer, D., Lupinacci, A., Parker, S., Valiev, R.Z., Shin, C., Choi, W. B., Hosemann, P., Investigation of specimen size effects by in-situ microcompression of equal channel angular pressed copper.*Materials Science and Engineering A* , 2016; **649** : p. 104-113.
53. Gussev, M., Busby, J.T., Field, K.G., Sokolov, M.A., Role of scale factor during tensile testing of small specimens, *Small Specimen Test Techniques: 6th Volume. 2015, West Conshohocken, PA: ASTM International* , Jan 29, 2014-Jan 31, 2014.
54. Chernobaeva, A.A., Medvedev, K.I., Zhurko, D.A., Kostromin, V.N., Skundin, M.A., Erak, D.Y., Mikhin, O.V., Scale factor of standard and mini Charpy specimens from VVER-1000 RPV materials.*International Journal of Pressure Vessels and Piping* , 2016;**145** : p. 23-28.
55. Callaghan, M.D., Humphries, S.R., Law, M., Bendeich, P., and Yeung, W.Y., Special testing equipment and validation of measurement methodologies for high temperature low cycle fatigue testing of miniature metallic specimens. *Experimental Mechanics* , 2016;**56** (6): p. 1039-1050.
56. Frederick, C.O., and Armstrong, P.J., A mathematical representation of the multiaxial Bauschinger effect. *Materials at High Temperatures* **,** 2007; **24** (1): p. 11-26.
57. Hyde, T.H., Yehia, K.A. and Becker, A.A., Interpretation of impression creep data using a reference stress approach. *International Journal of Mechanical Sciences* , 1993; **35** (6): p. 451-462.
58. Chen, H., and Cai L.X., Theoretical model for predicting uniaxial stress-strain relation by dual conical indentation based on equivalent energy principle, *Acta Materialia* , 2016; **121** , p. 181-189.
59. Sweeney, C.A., O'Brien, B., Dunne, F.P.E., McHugh, P.E., Leen, S.B., Strain-gradient modelling of grain size effects on fatigue of CoCr alloy. *Acta Materialia* , 2014; **78** : p. 341-353.
60. Barrett, R.A., P.E., O'Donoghue, and Leen, S.B., An improved unified viscoplastic constitutive model for strain-rate sensitivity in high temperature fatigue. *International Journal of Fatigue* , 2013;**48** : p. 192-204.
61. Nieslony, A., Chalid, D., Kaufmann, H., Krug, P., New method for evaluation of the Manson–Coffin–

Basquin and Ramberg–Osgood equations with respect to compatibility. *International Journal of Fatigue* , 2008; **30** (10-11): p. 1967-1977.

62. Kyaw, S.T., Rouse, J.P., Lu, J.W., Sun, W., Determination of material parameters for a unified viscoplasticity-damage model for a P91 power plant steel, *International Journal of Mechanical Science* , 2016;**115-116** , p. 168-179.
63. Li, D.H., Li, M., Shang D.G., Gupta, A., Sun, W., Physically-based modeling of cyclic softening and damage behaviors for a martensitic turbine rotor material at elevated temperature. *International Journal of Fatigue* , 2021; **142** : 105956.
64. Rae, Y., Guo, X., Benaarbia, A., Neate, N., Sun, W., On the microstructural evolution in 12% Cr turbine steel during low cycle fatigue at elevated temperature. *Materials Science and Engineering A* , 2020; **773** : 138864.
65. Zhang, B., Song, Z.M., Lei, L.M., Kang, L., Zhang, G.P., Geometrical scale-sensitive fatigue properties of Ti-6.5Al-3.5Mo-1.5Zr-0.3Si alloys with a/β lamellar microstructures, *Journal of Materials Science & Technology* , 2014; **30** (12), p.1287-1288.
66. Wan, H.Y., Chen, G.F., Li, C.P., Qi, X.B., Zhang, G.P., Data-driven evaluation of fatigue performance of additive manufactured parts using miniature specimens, *Journal of Materials Science & Technology* , 2019; **35** , p. 1137-1146.